Published March 2, 2009

Requirements for NuMA in maintenance and establishment of mammalian spindle poles

Alain D. Silk,[1,2] Andrew J. Holland,[1,2] and Don W. Cleveland[1,2]

[1]Ludwig Institute for Cancer Research and [2]Department of Cellular and Molecular Medicine, University of California, San Diego, La Jolla, CA 92093

Microtubules of the mitotic spindle in mammalian somatic cells are focused at spindle poles, a process thought to include direct capture by astral microtubules of kinetochores and/or noncentrosomally nucleated microtubule bundles. By construction and analysis of a conditional loss of mitotic function allele of the nuclear mitotic apparatus (NuMA) protein in mice and cultured primary cells, we demonstrate that NuMA is an essential mitotic component with distinct contributions to the establishment and maintenance of focused spindle poles. When mitotic NuMA function is disrupted, centrosomes provide initial focusing activity, but continued centrosome attachment to spindle fibers under tension is defective, and the maintenance of focused kinetochore fibers at spindle poles throughout mitosis is prevented. Without centrosomes and NuMA, initial establishment of spindle microtubule focusing completely fails. Thus, NuMA is a defining feature of the mammalian spindle pole and functions as an essential tether linking bulk microtubules of the spindle to centrosomes.

Introduction

The mitotic spindle is a bipolar array of microtubules required for the alignment and segregation of chromosomes during mitosis. The poles of the spindle are major focal points for the minus ends of spindle microtubules and serve as the final destination for chromosomes segregated in anaphase (Compton, 1998). In animal somatic cell mitosis, spindle poles are coincident with centrosomes, the major cellular microtubule-organizing structures. However, centrosomes are not required for the formation of the spindle or the pole. In vitro, DNA-coated beads catalyze the formation of bipolar microtubule spindles in acentrosomal *Xenopus laevis* egg extracts (Heald et al., 1996). Additionally, bipolar spindles also form in somatic mitotic cells in which centrosomes have been destroyed by laser ablation or prevented from forming normally by depletion of essential centrosomal components (Khodjakov et al., 2000; Mahoney et al., 2006). Previous studies in *Xenopus* extracts in vitro have established a role for the abundant spindle pole–localized nuclear mitotic apparatus (NuMA) protein in centrosome-independent spindle pole formation (Heald et al., 1996; Merdes et al., 2000). However, the relative contributions of NuMA and centrosomes in the establishment and maintenance of spindle pole integrity remain to be determined.

The attachment and movement of chromosomes on the mitotic spindle is mediated by kinetochore fibers, bundles of microtubules that link spindle poles to the kinetochores of each chromosome. Microtubules are nucleated in both a centrosome-dependent and -independent manner. Many are initiated directly at the pole by γ-tubulin–dependent nucleation, whereas others are nucleated adjacent to kinetochores through the local activation of components such as Tpx2 (Tulu et al., 2006). In the mitotic cytoplasm, these components are inactive as the result of binding to the importins but can be released by a chromosome-generated gradient of Ran-GTP (Gruss and Vernos, 2004). Under these conditions, microtubules nucleated in the vicinity of kinetochores are elongated and captured by centrosomal microtubules (Dasso, 2001; Khodjakov et al., 2003; Maiato et al., 2004). How these kinetochore-associated bundles are captured and focused toward centrosomes has not been determined. In addition, the means for sustained anchoring of kinetochore fibers at spindle poles and the role of centrosomes in both active focusing and the maintenance of spindle pole integrity are not established.

NuMA, along with cytoplasmic dynein, has been proposed to participate in focusing microtubules toward the poles of the mitotic spindle and physically tethering centrosomes to

Correspondence to Don W. Cleveland: dcleveland@ucsd.edu

Abbreviations used in this paper: 4-OHT, 4-hydroxytamoxifen; CENP-E, centromere protein E; ER^{TM}, estrogen receptor tamoxifen mutant; ES, embryonic stem; Flp, flipase; FRT, Flp recombinase target; GAPDH, glyceraldehyde 3-phosphate dehydrogenase; MEF, mouse embryo fibroblast; NuMA, nuclear mitotic apparatus; qPCR, quantitative PCR; STLC, S-trityl-L-cysteine; VAchT, vesicular acetylcholine transporter.

Supplemental Material can be found at:
http://jcb.rupress.org/content/suppl/2009/03/02/jcb.200810091.DC1.html

The Rockefeller University Press $30.00
J. Cell Biol. Vol. 184 No. 5 677–690
www.jcb.org/cgi/doi/10.1083/jcb.200810091

Published March 2, 2009

spindle microtubules (Merdes et al., 1996; Khodjakov et al., 2003). The foundation for our current mechanistic understanding of the role for NuMA during mitosis was established by work in cell-free extracts. Compared with typical mammalian spindles, those formed in *Xenopus* egg extracts are much larger, undergo substantially greater microtubule flux, and have limited astral microtubules and no cortical attachments (Ganem and Compton, 2006). Furthermore, spindles formed in egg extracts rely significantly more on a gradient of Ran-GTP emanating from chromosomes to contribute to spindle assembly and have relatively few bundled microtubules comprising kinetochore fibers (Kalab et al., 2002, 2006).

Investigations of NuMA function in mammalian mitosis have previously used antibody microinjection approaches, which have yielded contradictory outcomes. An early study reported spindle collapse to monopolarity (Yang and Snyder, 1992), and subsequent efforts demonstrated unfocused spindle poles and an extended mitotic delay (Gaglio et al., 1995). The difficulty in using siRNA to remove the abundant and long-lived NuMA protein has confounded strategies to determine mitotic NuMA function in the mammalian context (Elbashir et al., 2001; Chang et al., 2005). In addition, during interphase, NuMA accumulates in the nucleus, where it has been proposed to participate in aspects of nuclear structure and/or function, which might also be disrupted during extended siRNA treatment (Merdes and Cleveland, 1998; Harborth et al., 1999). To specifically test the principles of mammalian spindle assembly, particularly the mechanisms of spindle pole focusing and the maintenance of pole integrity, we now use gene replacement to engineer mice and cells in which NuMA's mitotic function can be selectively disrupted by administration of the small molecule 4-hydroxytamoxifen (4-OHT). Using this system, we demonstrate that NuMA is essential for early embryogenesis and cellular proliferation. During the first mitosis after inactivation of NuMA, spindles initially form with microtubules focused at centrosomes. However, subsequent to initial spindle assembly and upon generation of spindles forces, centrosome–spindle attachment is uncoupled. As a consequence, kinetochore fibers defocus, and centrosomes fail to maintain and reestablish connection with the spindle. Surprisingly, chromosome segregation is largely intact even without NuMA anchoring of kinetochore fibers to centrosomes. From these findings, we propose that NuMA is essential to maintain centrosome attachments to kinetochore fibers in mammalian mitosis and suggest that NuMA functions redundantly with centrosomes for initial focusing of microtubules at spindle poles.

Results

Creation of mice with a conditional exon 22 deletion allele of NuMA

Immunoblotting of extracts from a panel of mouse tissues indicated that NuMA was expressed at similar levels in most tissues examined (Fig. S1 A, available at http://www.jcb.org/cgi/content/full/jcb.200810091/DC1). In contrast, Mad2, BubR1, and centromere protein E (CENP-E), which are thought to be primarily or exclusively functional during mitosis, were only detected in the testes and spleen, which contain large numbers of dividing cells. Expression of the nuclear proteins lamin A and C was detected in all tissues examined and closely mirrored the expression of NuMA (Fig. S1 A). Examination of NuMA localization by immunostaining of terminally differentiated motor or Purkinje neurons demonstrated that NuMA was exclusively nuclear but excluded from nucleoli (Fig. S1 B). The near-ubiquitous expression pattern and accumulation of NuMA in nuclei of long-lived postmitotic cells supports the possibility of a nonmitotic interphase function of NuMA.

To test a mitotic role for NuMA without disrupting putative nuclear functions, we used gene targeting in mouse embryonic stem (ES) cells to create a conditional loss of mitotic function allele of NuMA. To do this, we identified an in-frame deletion within the NuMA gene that eliminated its microtubule binding without affecting intranuclear accumulation in interphase. The tubulin-binding domain of NuMA is comprised of an ~100 amino acid region in the C-terminal globular tail of NuMA, which interacts directly with tubulin in vitro and mediates its localization to spindle poles in vivo (Haren and Merdes, 2002). Mouse and human NuMA share 88% of amino acid identity in this domain, which is partially encoded by nucleotides comprising the 22nd exon of the mouse NuMA gene. We tested the localization of GFP-tagged versions of the 410 amino acid C-terminal globular tail of the mouse NuMA protein that were either wild-type or deleted for residues encoded by exon 22 (Fig. S2, A and B, available at http://www.jcb.org/cgi/content/full/jcb.200810091/DC1). The C-terminal tail was used to avoid association of tagged NuMA with endogenous NuMA through the central coiled-coil dimerization domain (Harborth et al., 1995). As expected, a wild-type NuMA tail fragment tagged with GFP localized appropriately to nuclei in interphase and was present in the crescent-shaped pattern typical of endogenous NuMA at spindle poles during mitosis (Fig. S2 C). The same GFP tail fragment, but lacking the 59 amino acids encoded by exon 22, was also nuclear during interphase but was severely compromised in localization to spindle poles during mitosis (Fig. S2, C and D).

Therefore, we generated a targeting construct designed to produce an allele of NuMA in which exon 22 could be conditionally deleted through the action of the Cre recombinase. Homologous recombination in mouse ES cells was used to flank exon 22 with loxP sites to create a $NuMA^{Neo}$ allele in which the Neo gene was itself deleteable by the action of the flipase (Flp) recombinase (Fig. 1 A). ES clones were screened by PCR and DNA blotting for homologous recombination at 5′ and 3′ ends of the exon 22 targeting construct, and multiple targeted clones were identified (Fig. 1, B–D). Two independently targeted ES cell lines were used to generate mice. These animals were crossed to an Flp-enhanced deleter strain (Rodriguez et al., 2000) to remove the Flp recombinase target (FRT)–flanked neomycin gene from intron 22, thereby generating a conditional allele, $NuMA^{flox}$. Subsequent mating to the ZP3-Cre mouse line expressing the Cre recombinase in the female germ line (Lewandoski et al., 1997) produced animals heterozygous for the NuMA deletion allele, $NuMA^{\Delta 22}$ (Fig. 1 A). Genotypes were confirmed using a three-primer PCR reaction capable of

Published March 2, 2009

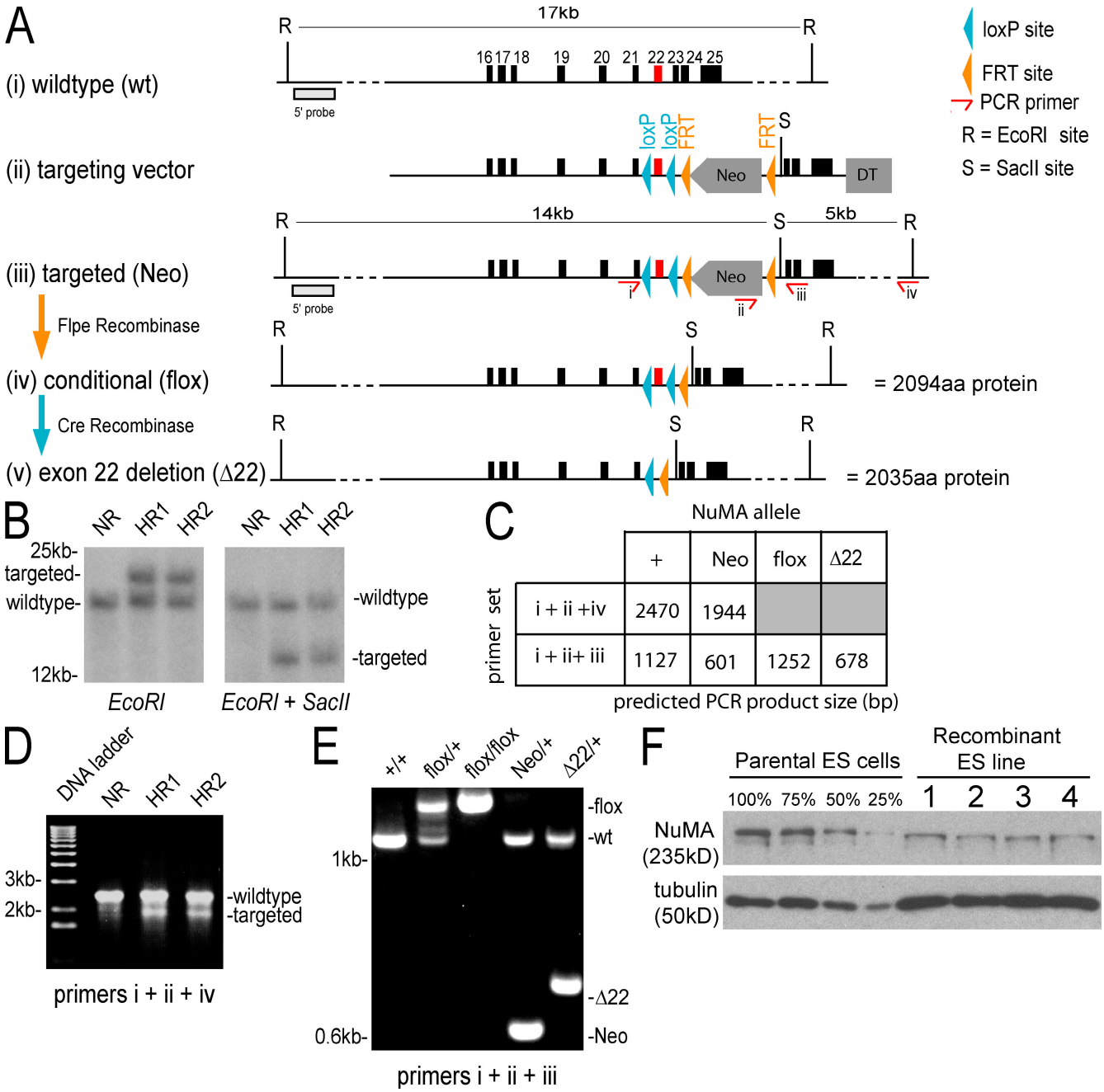

primer set	+	Neo	flox	Δ22
i + ii +iv	2470	1944		
i + ii+ iii	1127	601	1252	678

Figure 1. **Creation of conditional and disrupted NuMA alleles.** (A) Schematic representations of (i) a portion of the mouse NuMA gene including exons 16–25 and EcoRI restriction sites, (ii) the exon 22 targeting vector showing the neomycin resistance (Neo) and diphtheria toxin (DT) cassettes and placement of loxP and FRT sites, (iii) the structure of the correctly targeted allele with the introduced SacII restriction site and locations of genotyping primers, (iv) the conditional allele (flox) produced by Flp-enhanced recombinase–mediated recombination of FRT sites flanking Neo, and (v) the deletion allele (Δ) produced by Cre recombination of loxP sites surrounding exon 22. Red bars indicate exon 22. (B) Genomic DNA blotting from neomycin-resistant ES clones after digestion with either EcoRI alone or EcoRI and SacII in combination and hybridization with the 5′ probe shown in A. (C) Predicted PCR fragment sizes for wild-type, Neo, flox, and Δ22 alleles of NuMA using primer sets shown in A. (D) PCR products from neomycin-resistant ES clones using primers i, ii, and iv. (E) PCR products from mouse tail DNA using primers i, ii, and iii. (F) Four independently targeted ES clones and a dilution series blotted with antibodies to NuMA and tubulin. NR, nonrecombined; HR, homologously recombined.

distinguishing wild type and each of the engineered NuMA alleles (Fig. 1 E).

NuMA is essential for early development

Assessment of NuMA levels in ES cells and multiple tissues from mice heterozygous for the NuMA^{Neo} allele demonstrated a reduction in NuMA protein levels relative to wild-type cells and animals (Fig. 1 F), most likely the result of reduction in correctly spliced NuMA mRNA caused by the presence of the intronic neomycin cassette (Fig. S3, A–D, available at http://www.jcb.org/cgi/content/full/jcb.200810091/DC1). Taking advantage of this hypomorphic expression from NuMA^{Neo}, we tested

Published March 2, 2009

the requirement for NuMA in embryonic development and viability and found that the $NuMA^{Neo}$ allele could not be bred to homozygosity. No $NuMA^{Neo/Neo}$ live pups or early embryos were ever recovered (0/88 pups and 0/50 embryos; Table I). As expected, the conditional $NuMA^{flox}$ allele, produced by Flp-mediated removal of the neomycin marker, was readily bred to homozygosity (Table I). Like $NuMA^{Neo}$, $NuMA^{\Delta 22}$ (a 59–amino acid internal deletion) was embryonic lethal when homozygous (Table I). There was no evidence for NuMA haploinsufficiency or dominant effects that might be produced from either $NuMA^{Neo}$ or $NuMA^{\Delta 22}$; in crosses of mice heterozygous for either of these alleles, heterozygous and wild-type animals were produced in expected Mendelian ratios (Table I). Additionally, we aged cohorts of $NuMA^{Neo/+}$, $NuMA^{\Delta 22/+}$, and $NuMA^{flox/flox}$ mice for up to 18 mo, and in no case were any overt phenotypes observed. These observations demonstrate that NuMA is essential for one or more aspects of embryonic development and viability, $NuMA^{flox}$ encodes a functional protein, and $NuMA^{Neo}$ and $NuMA^{\Delta 22}$ are loss of function alleles.

Tamoxifen-regulated Cre-mediated deletion of NuMA exon 22

To examine cellular phenotypes resulting from NuMA loss of function and that might explain the requirement for NuMA in embryonic viability, cell lines were generated in which NuMA deletion could be induced by the addition of the small molecule 4-OHT. This was accomplished by crossing the $NuMA^{flox}$ allele into mice carrying a Cre–estrogen receptor tamoxifen mutant (ER^{TM}) transgene, which ubiquitously expresses the Cre recombinase fused to a mutated form of the estrogen receptor (Hayashi and McMahon, 2002). This receptor is insensitive to estrogen but binds with high affinity to the synthetic ligand 4-OHT. Binding of 4-OHT allows translocation of the receptor-Cre fusion from the cytoplasm to the nucleus, where Cre causes recombination between loxP sites.

Mating $NuMA^{flox/+}$,Cre-ER^{TM} to $NuMA^{flox/+}$ mice was used to obtain embryonic day 14.5 embryos that were wild type, heterozygous, or homozygous for the conditional NuMA allele and that also carried the Cre-ER^{TM} transgene. Mouse embryo fibroblasts (MEFs) were prepared from embryos of each genotype. To confirm that addition of 4-OHT would drive efficient recognition and recombination of loxP sites within the NuMA gene, contact-inhibited cells were treated with 4-OHT for 48 h in low serum. 4-OHT was subsequently washed out, and cells were maintained under growth arrest conditions for an additional 48 h to allow turnover of endogenous NuMA (Fig. 2 A). Multiple independent $NuMA^{flox/flox}$, Cre-ER^{TM} cell lines showed highly efficient deletion of the loxP-flanked region after 48 h of 4-OHT treatment (Fig. 2 B).

Quantification of recombination by quantitative PCR (qPCR) showed time and 4-OHT dose-dependent efficiency to exon 22 excision with a maximum effect observed after 48 h, resulting in a fibroblast population with 90% conversion of $NuMA^{flox}$ alleles to $NuMA^{\Delta 22}$ by day 4 (Fig. 2 C). Immunoblotting revealed that $NuMA^{\Delta 22}$ accumulated to a lower than wild-type level (Fig. 2 D). Remaining NuMA protein in $NuMA^{\Delta 22/\Delta 22}$ cells could not be eliminated by doubling the duration of cell cycle arrest after 4-OHT washout, suggesting that all wild-type NuMA had been completely turned over. As expected, the amino acids encoded by exon 22 were dispensable for nuclear accumulation of NuMA but were necessary for efficient spindle pole localization. We conclude that wild-type NuMA protein is absent from $NuMA^{\Delta 22/\Delta 22}$ MEFs 4 d after 4-OHT treatment and that the mutant protein accumulates to ~30% of the level of the wild-type NuMA polypeptide.

NuMA is required for proliferation of primary fibroblasts

To directly assess the consequences of preventing NuMA accumulation at spindle poles, population growth curves were generated for $NuMA^{+/+}$, $NuMA^{flox/+}$, and $NuMA^{flox/flox}$ MEFs, each carrying the Cre-ER^{TM} transgene. After treatment with 4-OHT to convert the $NuMA^{flox}$ allele to $NuMA^{\Delta 22}$, $NuMA^{+/+}$ and $NuMA^{+/\Delta 22}$ cells grew normally after release from low serum arrest, demonstrating that there are no dominant effects on cell cycle progression of mutant protein produced from the $NuMA^{\Delta 22}$ allele. Strikingly, $NuMA^{\Delta 22/\Delta 22}$ MEFs failed to increase in number after release from growth arrest (Fig. 2 E), demonstrating that removal of exon 22 results in cell-autonomous growth defects. These conclusions are consistent with cell-intrinsic defects, causing early embryonic lethality in $NuMA^{\Delta 22/\Delta 22}$ mice and the lack of dominant effects or haploinsufficiency observed in $NuMA^{\Delta 22/+}$ animals, which develop and age normally.

To determine whether loss of NuMA from spindle poles provoked extended delays in mitosis, as has been previously reported from antibody microinjection-mediated disruption of the

Table I. **Genotype incidence and frequencies of pups and embryos from $NuMA^{Neo/+}$, $NuMA^{flox/+}$, and $NuMA^{\Delta 22/+}$ heterozygous crosses**

Parental genotypes	Progeny	Progeny genotypes						
		+ +	Neo +	Neo Neo	flox +	flox flox	Δ22 +	Δ22 Δ22
Neo/+ × Neo/+	Pups[a]	23 (26%)	65 (74%)	0	NA	NA	NA	NA
	Embryos[b]	21 (42%)	29 (58%)	0	NA	NA	NA	NA
flox/+ × flox/+	Pups	34 (31%)	NA	NA	53 (47%)	25 (22%)	NA	NA
Δ22/+ × Δ22/+	Pups	14 (33%)	NA	NA	NA	NA	28 (67%)	0
	Embryos	7 (32%)	NA	NA	NA	NA	15 (68%)	0

Neo, $NuMA^{Neo}$; flox, $NuMA^{flox}$; Δ22, $NuMA^{\Delta 22}$; +, wild-type NuMA allele; NA, not applicable.

[a]Mouse pups were genotyped at postnatal day 21.

[b]Embryos were collected between embryonic days 9.5 and 14.5.

Published March 2, 2009

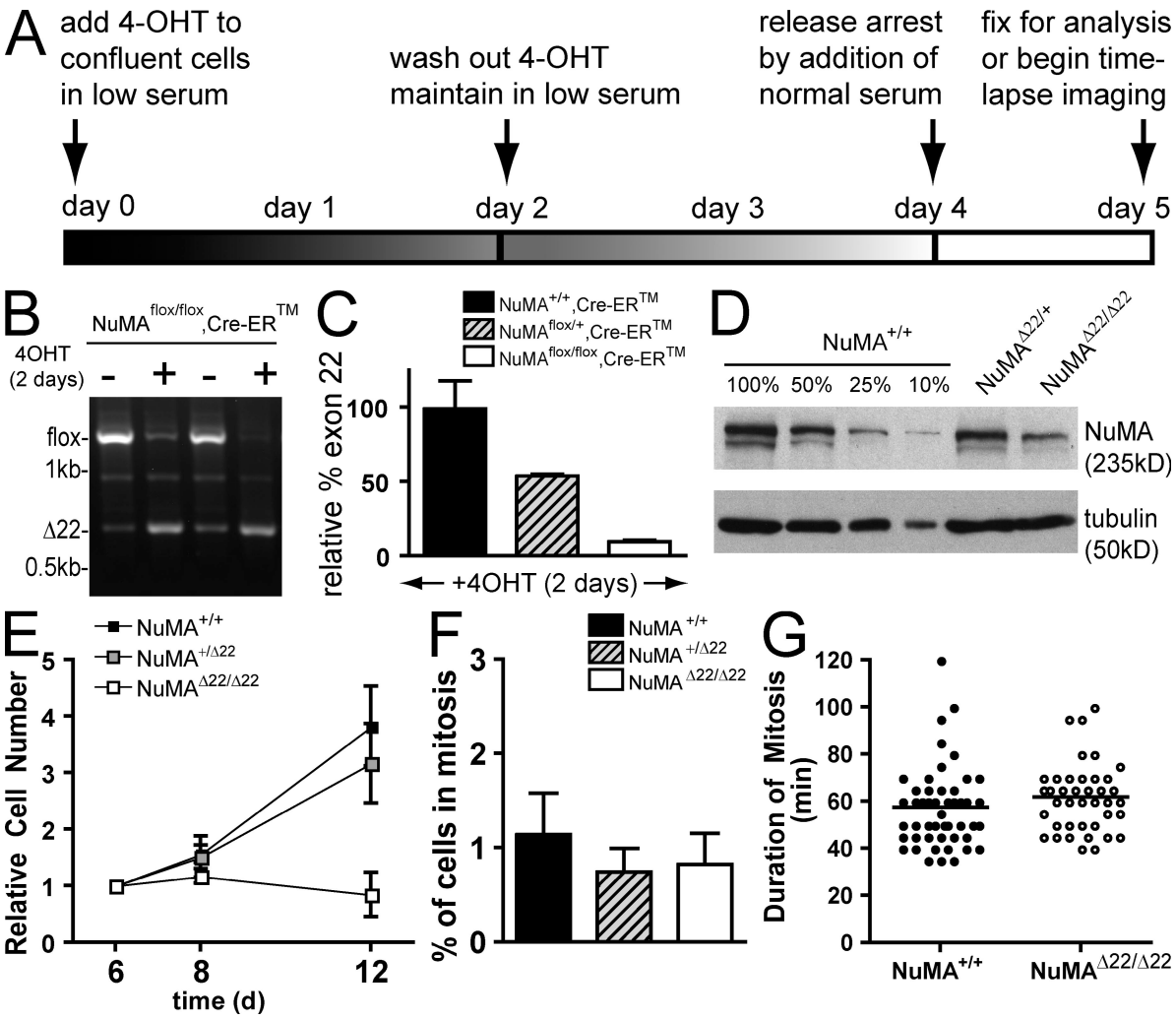

Figure 2. **Tamoxifen-induced disruption of NuMA inhibits proliferation of primary embryo fibroblasts.** (A) Timeline showing experimental design in which confluent primary cells are treated with 0.1 μM 4-OHT in 2% serum for 48 h. Cells were washed and maintained in 2% serum for 48 h before trypsinization and dilution into media containing 15% serum for subsequent analysis. (B) Conversion of $NuMA^{flox}$ to $NuMA^{\Delta 22}$ in two independent primary $NuMA^{flox/flox}$ cell lines carrying the Cre-ER^{TM} transgene. Recombination was monitored by PCR 48 h after treatment with 4-OHT. (C) qPCR using primers within the floxed region of NuMA was used to measure the efficiency of Cre-mediated recombination in the genomic DNA of fibroblasts. (D) Immunoblotting of NuMA and tubulin in $NuMA^{flox/flox}$,Cre-ER^{TM} and a dilution series of $NuMA^{+/+}$,Cre-ER^{TM} fibroblasts at day 4 of the experimental timeline. (E) Growth curves of primary fibroblasts after 4-OHT–mediated NuMA deletion; n = 3–4 experiments per cell line. Time in days follows timeline shown in A. (F) Mitotic index of primary MEFs treated with 4-OHT. For each genotype, >2,000 cells were counted in two separate cell lines. (G) Duration of mitosis in wild-type ($^{+/+}$, Cre) and NuMA-disrupted ($^{flox/flox}$, Cre) immortalized embryo fibroblasts. Results represent the mean of two independent experiments. Error bars represent SEM.

protein, the mitotic index of $NuMA^{\Delta 22/\Delta 22}$, $NuMA^{\Delta 22/+}$, and $NuMA^{+/+}$ MEFs was determined (Gaglio et al., 1995). There was no increase in the percentage of cells in mitosis after NuMA disruption (Fig. 2 F). Mitotic timing was reexamined even more directly in $NuMA^{+/+}$,Cre-ER^{TM} and $NuMA^{flox/flox}$,Cre-ER^{TM} immortalized fibroblasts, which were treated with 4-OHT, and the duration of mitosis was determined by phase-contrast time-lapse microscopy. After 4-OHT treatment, $NuMA^{flox}$ was converted to $NuMA^{\Delta 22}$ with the same efficiency as seen in primary cells. Mitosis was defined as the period between the first stage of cell rounding and the point at which cells had completely flattened back onto the substrate. Consistent with the failure of NuMA disruption to alter mitotic index, no significant difference in the duration of mitosis was observed between $NuMA^{\Delta 22/\Delta 22}$ and control cells (Fig. 2 G).

Spindle defects caused by loss of NuMA function

Despite normal timing of progression through mitosis, $NuMA^{\Delta 22/\Delta 22}$ primary cells displayed obvious spindle defects, most striking of which was the detachment of microtubule-nucleating structures from the ends of mitotic spindles. Costaining metaphase spindles with a γ-tubulin antibody provided strong evidence that the dissociated structures were bona fide centrosomes (Fig. S4 A, available at http://www.jcb.org/cgi/content/full/jcb.200810091/DC1). In some cells, spindles retained focused arrays of microtubule ends despite having no closely associated centrosome, whereas in others, even poles with associated centrosomes lacked a discernable microtubule focus (Fig. 3 A). Greater than 50% of metaphase-like cells in the $NuMA^{\Delta 22/\Delta 22}$ population had at least one centrosome that was clearly not

Published March 2, 2009

associated with a spindle pole (apolar centrosome), and a similar frequency had at least one pole in which microtubules did not converge to a single focal point (unfocused kinetochore fibers; Fig. 3 C). These phenotypes contrasted sharply with metaphases observed in wild-type and NuMA$^{+/\Delta22}$ cells, which showed typical spindle architecture with focused microtubule arrays terminating near centrosomes (Fig. 3, A and C). In addition to centrosome–spindle coupling and microtubule-focusing defects, metaphase spindle lengths in MG132-arrested NuMA$^{\Delta22/\Delta22}$ cells were on average 30% longer than either wild-type or NuMA$^{+/\Delta22}$ controls (Fig. 3 D).

The spindle defects observed in NuMA$^{\Delta22/\Delta22}$ cells were also present in anaphase (Fig. 3 B). However, immunostaining of unperturbed fibroblasts with a cyclin B1 antibody confirmed that the apolar centrosome and pole-defocusing phenotypes in NuMA$^{\Delta22/\Delta22}$ fibroblasts occurred before anaphase onset (Fig. S4 B). In addition, cells arrested in metaphase by blocking cyclin B and securin degradation by treatment with the proteasome inhibitor MG132 showed similar spindle defects at high frequency, corroborating this interpretation (Fig. S4 A). Tension between sister kinetochores in pole-defocused spindles was reduced by ~33% compared with normal cells (Fig. 4, A and B), and chromosome alignment defects were observed more frequently in metaphase NuMA$^{\Delta22/\Delta22}$ than control NuMA$^{+/\Delta22}$ fibroblasts (Fig. 4, C and D). Therefore, spindles in NuMA$^{\Delta22/\Delta22}$ cells are deficient in their ability to apply or retain tension

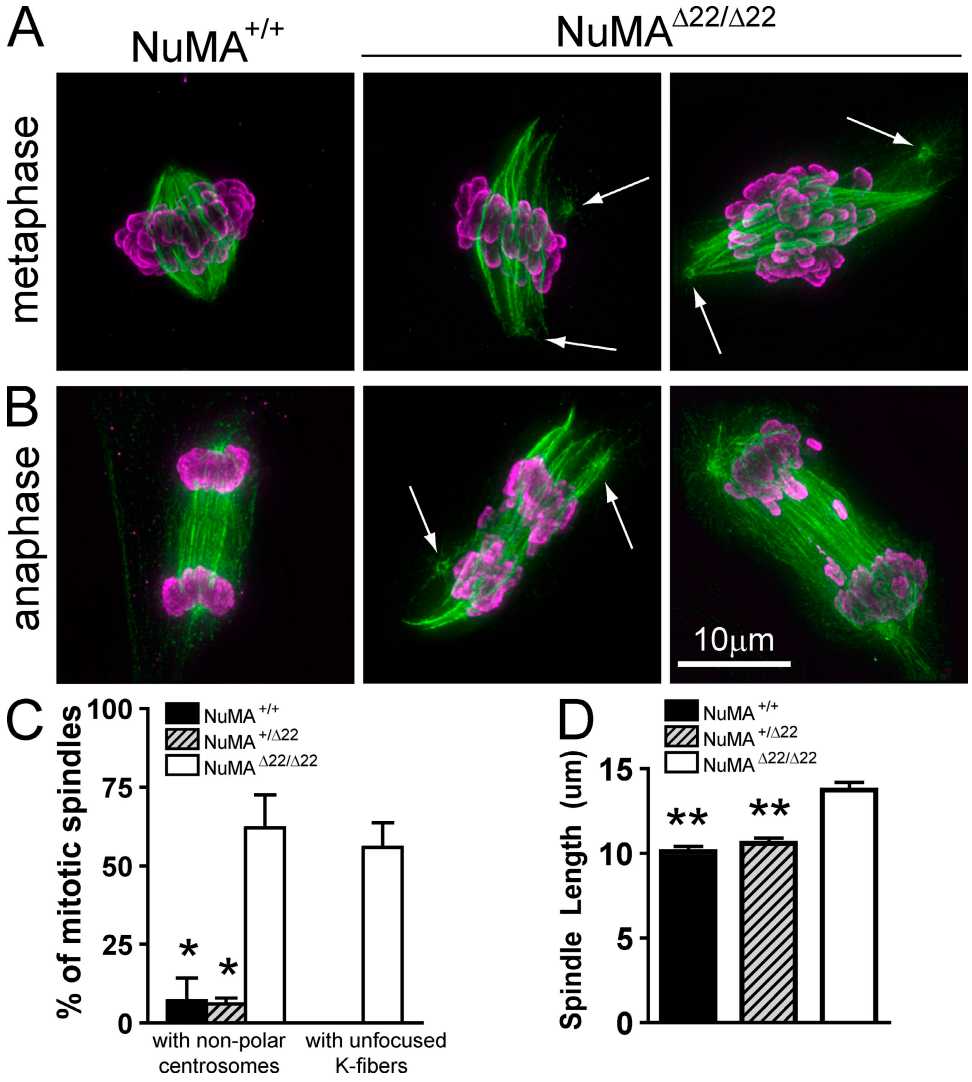

Figure 3. **Spindle defects in primary NuMA$^{\Delta22/\Delta22}$ fibroblasts.** Primary fibroblasts were processed for immunofluorescence on experimental day 5, as shown in Fig. 2 A. (A) Example of metaphase in a control cell (NuMA$^{+/+}$) and two exon 22–deleted (NuMA$^{\Delta22/\Delta22}$) primary fibroblasts. Arrows indicate centrosomes. (B) Anaphase in wild-type and two NuMA$^{\Delta22/\Delta22}$ primary cells. Each image represents a maximum intensity projection of a deconvolved series of z sections spanning the entire cell in 0.2-μm intervals. Arrows indicate centrosomes. Tubulin is shown in green, and phosphorylated histone H3 is shown in purple. (C) Frequencies of spindle–centrosome dissociation and pole splaying defects seen in control and NuMA-depleted metaphase cells. Cells were scored as phenotypic if at least one centrosome was nonpolar or at least one pole displayed an obvious lack of microtubule focusing. Two independent cell lines were examined per genotype, with >50 cells counted for NuMA$^{+/+}$ and >130 cells for each of NuMA$^{+/\Delta22}$ and NuMA$^{\Delta22/\Delta22}$ fibroblasts. (D) Spindle length in MG132-arrested primary fibroblasts measured as the linear distance between spindle poles or the approximate position of most spindle microtubule ends in defocused poles. At least 20 spindles per genotype were examined. *, $P < 0.01$ using Bonferroni's multiple comparison test and compared with NuMA$^{\Delta22/\Delta22}$; **, $P < 0.001$. Error bars indicate SEM.

Published March 2, 2009

across sister kinetochores and align chromosomes in a metaphase alignment.

Spindle abnormalities were likely not caused by a failure of the dynein–dynactin complex to localize appropriately. A component of dynactin, p150, localized to centrosomes independent of spindle attachment, suggesting that failure of centrosome–spindle coupling and loss of kinetochore fiber focusing did not result from mislocalization of dynein–dynactin, the major mitotic binding partner of NuMA (Fig. S4 C). Cold treatment to preferentially depolymerize dynamic microtubules confirmed that kinetochore fibers remained stably attached to kinetochores in NuMA-disrupted cells even when completely defocused at poles and detached from centrosomes (Fig. S4 D).

From these results, we conclude that spindle pole integrity is defective in the absence of NuMA and more specifically that NuMA is required at spindle poles to couple centrosomes to kinetochore fibers. We also note that although kinetochore–microtubule attachments are apparently intact, tension across sister kinetochores is reduced, and chromosome alignment is defective in NuMA$^{\Delta 22/\Delta 22}$ cells.

Spindle bipolarization precedes centrosome detachment in the absence of NuMA

The displacement of centrosomes from kinetochore fibers in metaphase could arise either from an initial failure of NuMA$^{\Delta 22/\Delta 22}$ cells to focus microtubules at the poles of the spindle or from an inability to maintain centrosome attachment to a fully formed spindle. To distinguish these possibilities, we followed spindle formation and mitotic progression in live NuMA$^{\Delta 22/\Delta 22}$ MEFs. Primary cells were transduced with a retrovirus encoding tubulin-YFP 2 d before the initiation of Cre recombinase activity with 4-OHT and arrest in G0/G1 with low serum. Cells were subsequently released from arrest and filmed by time-lapse fluorescence microscopy. NuMA$^{+/\Delta 22}$ cells always formed bipolar spindles and maintained centrosomes at spindle poles throughout mitosis (6/6 morphologically normal spindles; Fig. 5 A; and Video 1, available at http://www.jcb.org/cgi/content/full/jcb.200810091/DC1). In contrast, NuMA$^{\Delta 22/\Delta 22}$ fibroblasts exhibited a high frequency of pole defocusing and centrosome detachment phenotypes (9/13 spindles aberrant) (Fig. 5 B). Live cell imaging showed clearly that in NuMA$^{\Delta 22/\Delta 22}$ cells, microtubules can establish focusing at centrosomes during the initial

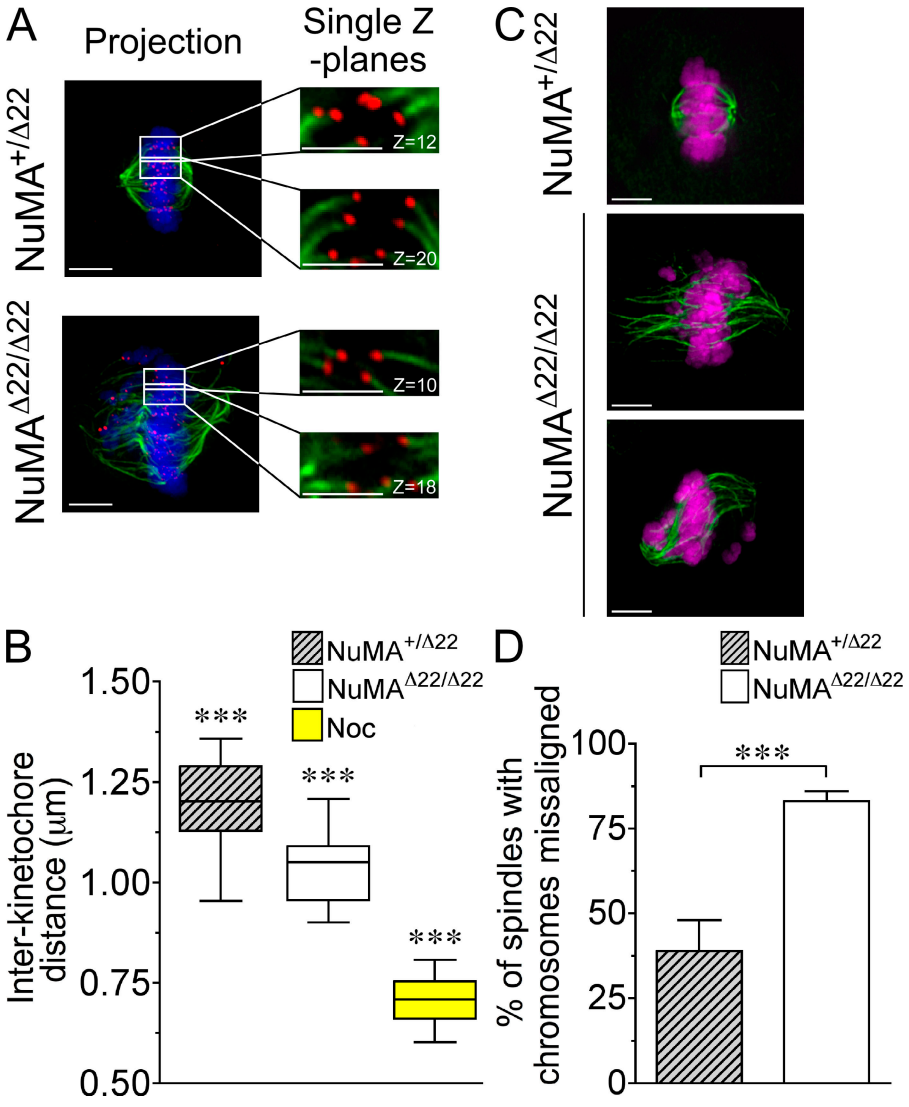

Figure 4. **Reduced spindle tension and efficiency of chromosome alignment in the absence of NuMA.** (A) Distance between sister kinetochores in cells arrested in metaphase with MG132 and incubated on ice for 10 min to selectively depolymerize nonkinetochore fiber microtubules. Images represent maximum intensity projections of a deconvolved series of z sections spanning the entire cell in 0.2-µm intervals (projection) or single deconvolved z sections. Kinetochore pairs were identified in single z sections by the relative positioning of kinetochores and orientation of associated kinetochore fibers. Blue, DNA; green, microtubules; red, kinetochores. Bars: (left) 5 µm; and (right) 2.5 µm. (B) Interkinetochore distances of paired sister chromatids in NuMA$^{+/\Delta 22}$, NuMA$^{\Delta 22/\Delta 22}$, and nocodazole (Noc)-treated control cells. The boxes represent the interquartile (middle 50%), and the whiskers represent the full range. Horizontal lines represent the median value. (C) Examples of NuMA$^{+/\Delta 22}$ cells with fully aligned chromosomes and NuMA$^{\Delta 22/\Delta 22}$ fibroblasts with chromosome alignment defects. Cells were treated as in A and processed for immunofluorescence to visualize DNA (purple) and tubulin (green). Bars, 5 µm. (D) Percentage of spindles showing chromosome alignments defects. ***, $P < 0.0001$. Error bars indicate SEM.

Published March 2, 2009

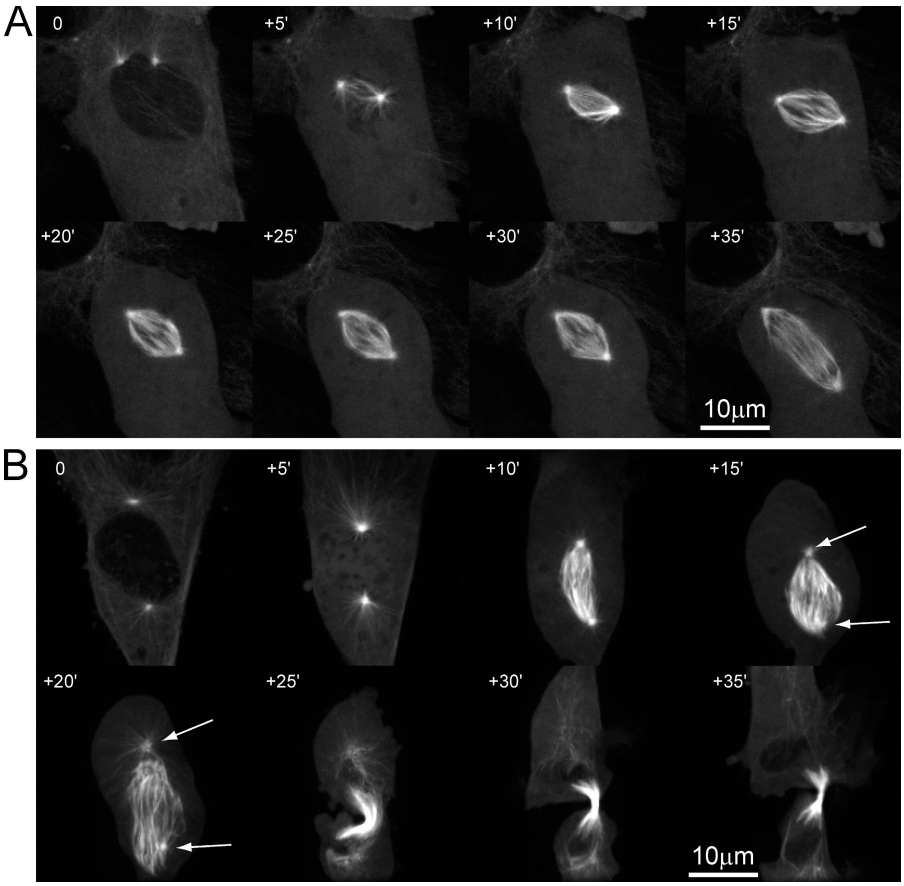

Figure 5. **Bipolar spindle formation precedes centrosome detachment in the absence of mitotic NuMA function.** (A and B) Selected images from videos of primary embryo fibroblasts transduced with retrovirus encoding tubulin-YFP, either heterozygous (A; Video 1, available at http://www.jcb.org/cgi/content/full/jcb.200810091/DC1) or homozygous (B; Video 2) for NuMA$^{\Delta 22}$, undergoing the first mitosis after 4-OHT treatment and release from growth arrest. Arrows indicate centrosomes, and each time point shows a maximum intensity projection of five confocal fluorescence z sections acquired in 2-μm intervals.

stages of spindle assembly but that as cells progress through mitosis, maintenance of centrosome–spindle coupling is lost, and poles subsequently defocus.

Despite these defects, completion of mitosis appeared normal, daughter cells formed morphologically normal nuclei, and cytokinesis, including abscission, also occurred (Video 2, available at http://www.jcb.org/cgi/content/full/jcb.200810091/DC1). We also measured the duration of mitosis in tubulin-YFP–expressing MEFs, which we defined as the length of time between nuclear envelope breakdown and the first observable stage of midbody formation. Consistent with our previous observations, mitotic timing was similar for control (33 ± 9 min, $n = 6$) and NuMA$^{\Delta 22/\Delta 22}$ cells that experienced spindle defects (27 ± 5 min, $n = 5$). Additionally, the kinetics of spindle bipolarization were similar in control (12 ± 4 min, $n = 6$) and phenotypic NuMA$^{\Delta 22/\Delta 22}$ cells (13 ± 3 min, $n = 5$). These observations indicate that loss of NuMA function during mitosis does not prevent the initial timely establishment of focused bipolar spindles but results in centrosome loss from the spindle poles before anaphase followed by microtubule defocusing. Surprisingly, despite these defects, bulk chromosome segregation proceeds largely as normal in NuMA$^{\Delta 22/\Delta 22}$ cells (Fig. 3 B and Video 2).

The NuMA$^{\Delta 22}$ allele supports potential interphase functions of NuMA

The ability of NuMA$^{\Delta 22/\Delta 22}$ cells to enter mitosis and the spindle phenotypes observed were consistent with specific defects in spindle pole integrity. To confirm that a potential nuclear defect in NuMA$^{\Delta 22/\Delta 22}$ cells was not responsible for the subsequent mitotic deficits, we performed an in vivo test for retention of nuclear function of the NuMA$^{\Delta 22}$ protein. To do this, wild-type NuMA was replaced with NuMA$^{\Delta 22}$ protein in spinal cord motor neurons, a cell type in which NuMA is known to be present in nuclei in adult neurons (Fig. S1 B). These cells were chosen for two reasons: first, defects in motor neuron function give rise to characteristic and easily scorable motor deficits, including gait alterations and paralysis. Second, the lifetimes of individual neurons extend for the full life span of the organism, allowing access to any age-dependent features of loss of interphase NuMA function.

NuMA was deleted specifically from motor neurons by crossing the NuMA^{flox} allele with animals carrying the vesicular acetylcholine transporter (VAchT)–Cre transgene. This transgene has previously been demonstrated to direct Cre recombinase expression exclusively in motor neurons after the final division of motor neuron progenitors, ensuring that any phenotypes would arise exclusively from postmitotic loss of NuMA (Misawa et al., 2003). NuMA$^{flox/flox}$,VAchT-Cre, NuMA$^{+/flox}$,VAchT-Cre, and NuMA$^{flox/flox}$ littermate controls were obtained, and animals of all genotypes and genders were produced in expected Mendelian ratios. Activity of the Cre recombinase and restriction of expression to motor neurons in VAchT-Cre mice was confirmed by mating to the ROSA26R reporter strain (Soriano, 1999). Examination of spinal cord and sagittal brain sections from VAchT-Cre,ROSA26R mice for β-galactosidase activity confirmed that Cre expression

Published March 2, 2009

was restricted to motor neurons (Fig. S5 A, available at http://www.jcb.org/cgi/content/full/jcb.200810091/DC1).

Extensive visual observation demonstrated that $NuMA^{flox/flox}$, VAchT-Cre animals showed no behavioral defects indicative of motor neuron dysfunction, even at up to 2 yr of age. Weight gain was also similar in control and $NuMA^{flox/flox}$,VAchT-Cre mice, providing no evidence for motor neuron dysfunction or muscle denervation (Fig. S5 B). Finally, counting of cresyl violet–stained motor neuron cell bodies in spinal cord sections of 200-d-old animals revealed no effect on motor neuron numbers (Fig. S5 C). Thus, the exon 22–deleted mutant complements all potential nuclear functions of NuMA and does so for extended periods in vivo. Alternatively, NuMA may perform limited or redundant interphase functions in these cells.

NuMA is required for the maintenance of centrosome–spindle coupling in bipolar spindles under tension

Live imaging of tubulin-YFP–marked spindles in unperturbed fibroblasts demonstrated that in the absence of NuMA, initial microtubule focusing at the pole appeared normal. This strongly supports a maintenance rather than establishment role for NuMA in the attachment of centrosomes to kinetochore fibers. To further test this, we arrested NuMA wild-type, $NuMA^{+/\Delta22}$, and $NuMA^{\Delta22/\Delta22}$ cells in mitosis with the Eg5 inhibitor S-trityl-L-cysteine (STLC; Skoufias et al., 2006). Eg5 is a bipolar, homotetrameric, kinesin-related motor protein that is required during mitosis to both establish and maintain separation of centrosomes. It is thought to function by cross-linking and sliding apart antiparallel microtubules from opposing centrosomes, thereby pushing centrosomes apart (Kapitein et al., 2005). STLC inhibits activity of Eg5, causing collapse of bipolar spindles. Regardless of genotype, in the absence of STLC, monopolar spindles were observed with equally low frequency in all cell lines, but upon STLC treatment, all MEF cell lines produced a high frequency of monopolar spindles that appeared almost exclusively as chromosome rosettes surrounding a central γ-tubulin–positive pole (Fig. 6, A and B). This indicates that in monopolar spindles, centrosomes continue to dictate the location of spindle pole formation when NuMA function is disrupted. Furthermore, under these conditions, kinetochore fibers do not require NuMA for active focusing toward centrosomes.

Throughout the extended mitotic delay caused by treatment with STLC, centrosomes persisted at the center of monopolar spindles in $NuMA^{\Delta22/\Delta22}$ cells. How can this be reconciled with a maintenance role of NuMA in centrosome–spindle coupling? Relative to bipolar metaphase spindles, monopolar spindles have reduced tension forces acting between centrosomes and kinetochores. Thus, the spindle defects produced in cycling $NuMA^{\Delta22/\Delta22}$ cells likely reflect a requirement for NuMA in maintaining centrosomes at poles of spindles experiencing typical metaphase forces. To directly test this possibility, STLC was washed out from monopolar-arrested cells to reintroduce tension into spindles with kinetochore fibers focused toward a monopole. 1 h after release, cells were fixed for immunofluorescence. In control cells, anaphases always had one centrosome at each pole (Fig. 6 C). In contrast, $NuMA^{\Delta22/\Delta22}$ cells displayed anaphase figures in which chromosomes had segregated normally, but spindle poles were defocused, and centrosomes (detected as discrete foci of strong γ-tubulin staining) had failed to separate.

These results were corroborated by following the recovery of spindle bipolarity in retrovirally transduced α-tubulin-YFP–expressing fibroblasts. After release from STLC, control cells were uniformly observed to recover from monopolarity by separating centrosomes and forming bipolar spindles with well-focused poles (7/7 cells; Fig. 6 D; and Video 3, available at http://www.jcb.org/cgi/content/full/jcb.200810091/DC1). However, after the reestablishment of tension, $NuMA^{\Delta22/\Delta22}$ fibroblasts often formed spindles with one well-focused pole and one splayed spindle pole lacking a centrosome (8/13 cells; Fig. 6 D and Video 4). We conclude that mitotic NuMA function is required to maintain centrosome–spindle attachments under conditions in which tension is applied across the spindle.

Adjacent centrosomes that failed to separate in $NuMA^{\Delta22/\Delta22}$ cells were always initially observed at the spindle end with focused microtubules. As $NuMA^{\Delta22/\Delta22}$ cells progressed through mitosis, the paired centrosomes often dissociated from the pole. These cone-shaped spindles were not arrested monopolar spindles observed in profile because they uniformly proceeded into anaphase, indicating that mitotic checkpoint signaling was silenced. These data demonstrate that normal NuMA function is required for centrosome separation after recovery from a monopolar state. In addition, because the centrosome distal half of each NuMA-deficient spindle forms a splayed pole after release from STLC, we conclude that in the absence of centrosomes, NuMA is required for the establishment of microtubule focusing.

Stable kinetochore–microtubule interactions are required for centrosome separation after recovery from monopolarity

The aforementioned evidence demonstrates a requirement for NuMA in the physical tethering of centrosomes to kinetochore fibers and reveals the surprising finding that centrosome–spindle connections are required for centrosome separation after recovery from monopolarity. This finding has important implications for the mechanism of centrosome separation during reestablishment of spindle bipolarity in prometaphase. Therefore, we specifically tested whether stable microtubule–kinetochore attachments are also required for centrosome separation in recovering monopolar spindles. The Ndc80 complex, a heterotetramer composed of the Ndc80, Nuf2, Spc24, and Spc25 proteins, is a key component involved in the stable attachment of microtubule bundles at kinetochores (Cheeseman and Desai, 2005). To directly test the requirement for kinetochore–microtubule attachment in centrosome separation, we used siRNA to deplete Nuf2 in HeLa cells stably expressing fluorescently tagged tubulin and histone H2B (Fig. 7 A). These cells were arrested with monopolar spindles using STLC, the drug was removed, and time-lapse fluorescence microscopy was used to observe recovery of spindle bipolarity. 90 min after STLC washout, all but 3% of control siRNA-treated cells had separated their centrosomes and formed bipolar spindles. However, in the same period of time, 35% of Nuf2-depleted

Published March 2, 2009

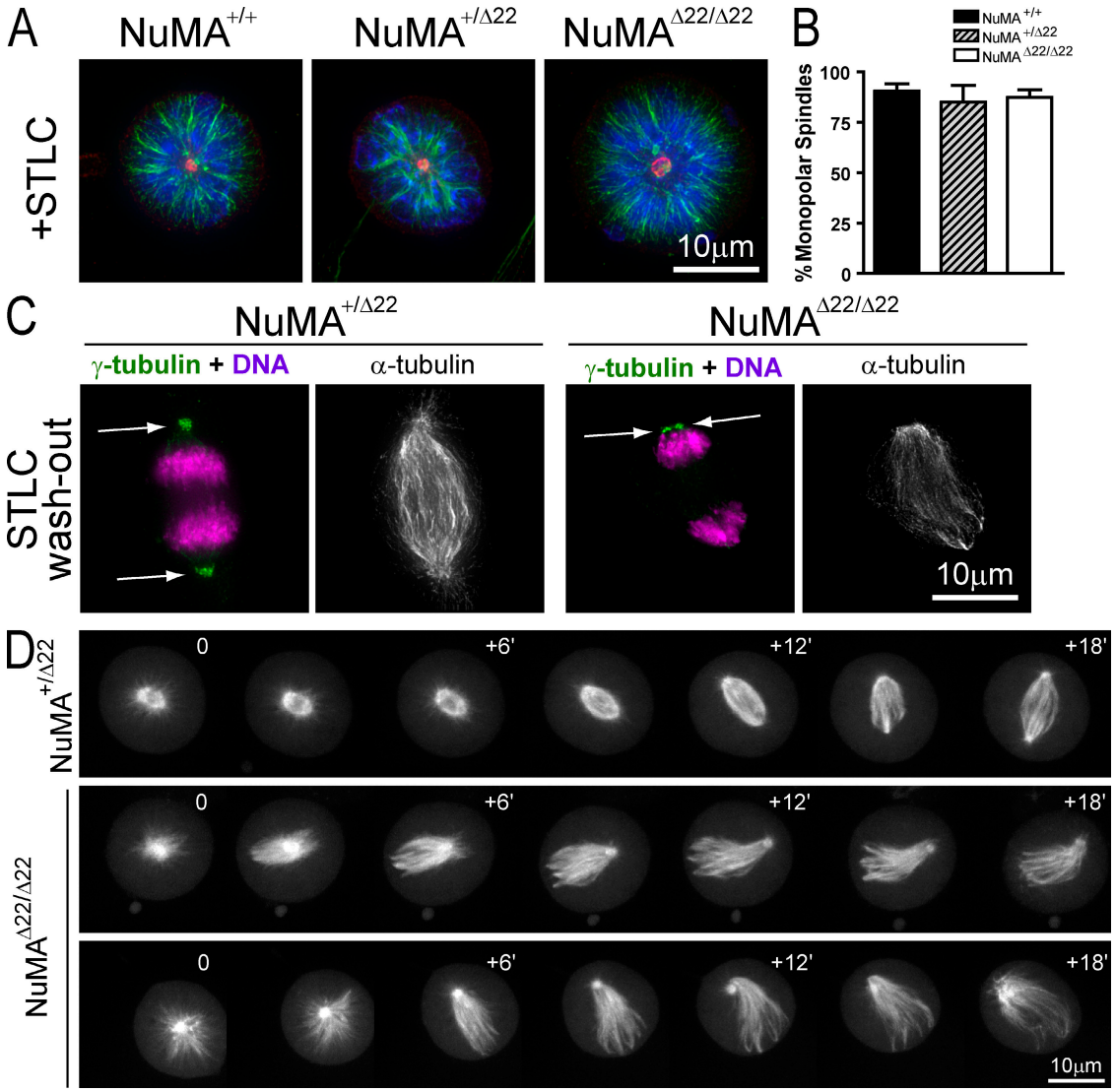

Figure 6. **Prometaphase centrosome separation and centrosome-independent spindle pole focusing require NuMA.** (A) Primary MEFs were arrested in mitosis by treatment with STLC and processed for immunofluorescence. Green, α-tubulin; blue, DNA; red, γ-tubulin. (B) Frequencies of monopolar spindles as shown in A. Two independent cell lines per genotype were used, and >200 mitoses per genotype were counted. (C) Anaphase in NuMA$^{+/\Delta22}$ control and NuMA$^{\Delta22/\Delta22}$ cells 1 h after washout of STLC. In merged images, DNA is shown in purple and γ-tubulin in green. Arrows indicate centrosomes. (D) Stills from videos of NuMA$^{+/\Delta22}$ (Video 3, available at http://www.jcb.org/cgi/content/full/jcb.200810091/DC1) and NuMA$^{\Delta22/\Delta22}$ (Video 4) primary embryo fibroblasts transduced with retrovirus encoding tubulin-YFP. Cells were arrested with STLC for 3–4 h and filmed after washout of the drug. Scoring for centrosome separation was performed blinded to genotype. Each time point shows a maximum intensity projection of 12 confocal fluorescence z sections acquired in 1-μm intervals. Error bars indicate SEM.

spindles failed to resolve their centrosomes and form bipolar spindles (Fig. 7, B and C). We conclude that efficient centrosome separation after recovery from monopolar spindles relies on the two-point attachment of kinetochore fibers at centrosomes and kinetochores.

Discussion

In this study, we describe the creation of a separation of function allele of NuMA by specific deletion of exon 22 of the mouse NuMA gene. Removal of exon 22 produces a mutant protein that is unable to efficiently localize to spindle poles during mitosis but is able to perform all essential interphase functions of NuMA. By combining inducible inactivation of this allele with a prolonged G0/G1 arrest, we were able to achieve nearly quantitative turnover of accumulated wild-type NuMA protein before the first mitotic division. Strikingly, we show that in the absence of functional NuMA, and despite apparently normal initial bipolar spindle formation, centrosomes are unable to maintain attachment to the ends of kinetochore fibers. The subsequent defocusing of microtubules at spindle poles reveals a distinct requirement for NuMA in the maintenance of mammalian centrosome–spindle attachments.

Mechanisms and maintenance of microtubule focusing at poles

A previous study has implicated a role for NuMA-mediated capture of kinetochore fibers in pole focusing (Khodjakov et al., 2003).

Published March 2, 2009

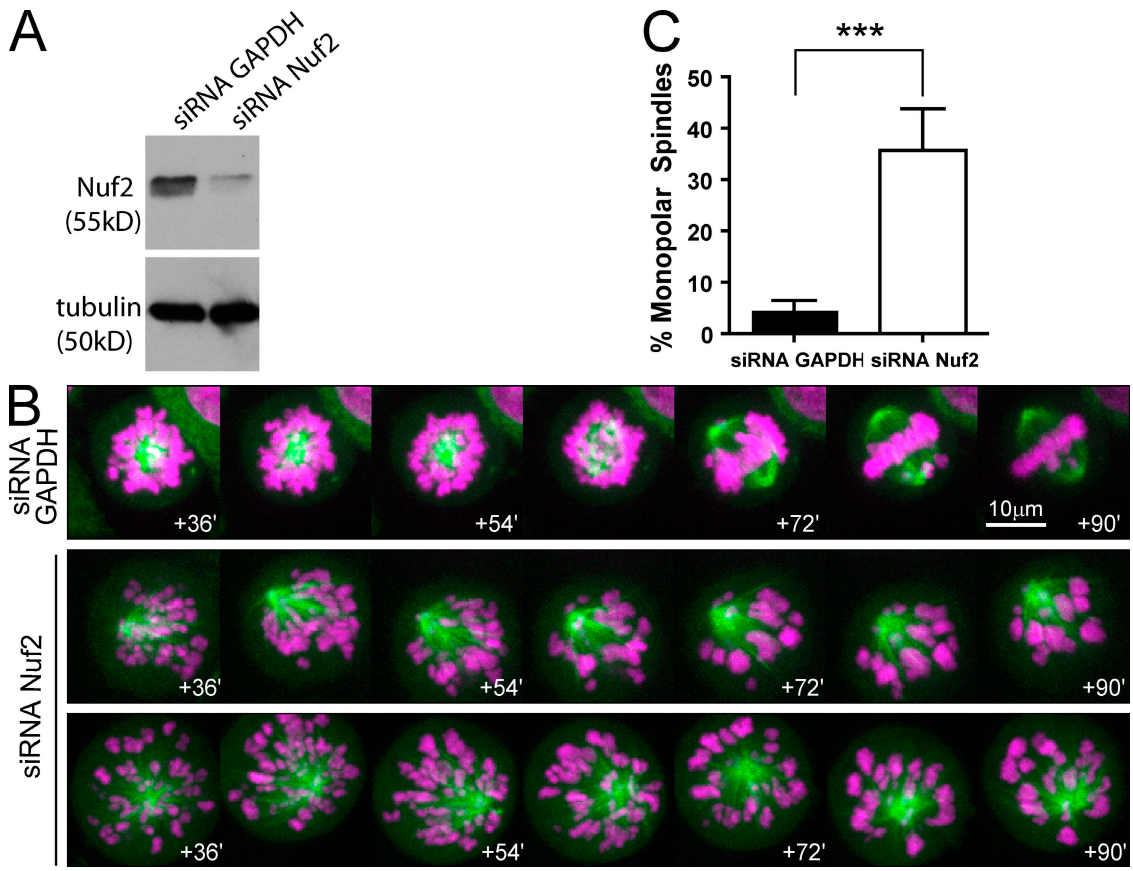

Figure 7. **Kinetochore–microtubule attachments are required for centrosome separation in prometaphase.** (A) Immunoblot of an extract of HeLa cells 48 h after transfection with siRNA oligos against glyceraldehyde 3-phosphate dehydrogenase (GAPDH) or Nuf2. (B) Still images from videos of HeLa cells coexpressing H2B–monomeric RFP and tubulin-YFP. Cells were transfected with siRNA oligos against GAPDH or Nuf2 and 48 h later were arrested with STLC. Time is given in minutes relative to STLC washout. Images are maximum intensity projections of five confocal z sections spaced 2 μm apart. Green, tubulin; purple, histone H2B. (C) Frequency of spindles that remained monopolar 90 min after release from STLC in cells treated with siRNA to GAPDH or Nuf2. Error bars represent the mean and SEM of three separate experiments; n = 192 cells GAPDH siRNA; n = 228 cells Nuf2 siRNA; ***, $P < 0.0001$ by Fisher's exact test.

This has been proposed to occur through the capture of kinetochore fibers by NuMA (Khodjakov et al., 2003), which itself is transported toward spindle poles, likely on centrosomal/astral microtubules by dynein (Merdes et al., 2000). However, centrosomes are not required for microtubule focusing or NuMA localization to spindle poles (Khodjakov et al., 2000). Our efforts in this study have extended this to demonstrate that in the absence of functional NuMA, initial bipolar spindle formation proceeds normally. However, after the establishment of tension across kinetochores, centrosomes subsequently detach from the spindle, and microtubules defocus. This demonstrates that NuMA is required to physically tether kinetochore fiber minus ends at the poles of bipolar spindles under tension and provides the first evidence that an essential function of NuMA during mitosis is in the maintenance and not establishment of mammalian centrosomal–spindle connections.

The normal initiation of bipolar spindle formation in the absence of NuMA suggests the existence of alternative processes involved in establishing focused spindle poles. These are likely to be dependent on the presence of centrosomes, which might function in cooperation with components such as HSET in mammals and Ncd in *Drosophila melanogaster* (Gordon et al., 2001; Goshima et al., 2005). This interpretation is corroborated by our observation that after recovery from monopolarity, microtubules in NuMA$^{\Delta 22/\Delta 22}$ fibroblasts are severely defocused in the acentrosomal spindle half. The formation of these monoastral, bipolar cone-shaped spindles provides clear evidence that NuMA is required for spindle pole focusing in the absence of centrosomes. Thus, NuMA and centrosomes function redundantly in establishing spindle poles by contributing independently to initial microtubule focusing. It is likely that mammalian acentrosomal spindle systems, including mouse oocytes, rely heavily on NuMA for the establishment of spindle poles, which is a question now testable with the NuMA$^{\Delta 22}$ allele.

Disruption of dynein function gives rise to defects similar to those we have observed in NuMA$^{\Delta 22/\Delta 22}$ MEFs, including centrosome–spindle uncoupling and, to a lesser extent, a mild degree of kinetochore fiber defocusing during metaphase (Heald et al., 1997; Goshima et al., 2005). In multiple contexts, dynein inhibition causes NuMA to redistribute from spindle poles to along the length of spindle microtubules. This suggests that a major function of spindle-localized dynein in mitosis may be to transport NuMA as a cargo to microtubule minus ends (Gaglio et al., 1997; Merdes et al., 2000). The rapid kinetics of

Published March 2, 2009

NuMA localization to spindle poles and the kinetochore fiber–independent nature of NuMA accumulation at poles (unpublished data) is consistent with this interpretation. Therefore, much of the phenotype caused by inhibition of dynein function may be a direct result of a failure to properly localize NuMA.

Function of Eg5 in prometaphase centrosome separation

In mitotic prophase before nuclear envelope breakdown, two duplicated centrosomes move across the nuclear envelope in a dynein-dependent manner to diametrically oppose each other in anticipation of bipolar spindle formation (Gonczy et al., 1999). Maintenance of centrosome separation after nuclear envelope breakdown requires activity of the plus end–directed motor Eg5, which acts to slide apart antiparallel microtubules that emanate directly from centrosomes. Inhibition of Eg5 activity causes centrosome collapse after nuclear envelope breakdown, triggering an extended mitotic delay (Kapitein et al., 2005; Skoufias et al., 2006). Surprisingly, we demonstrate that centrosome separation fails after restoration of Eg5 activity in monopolar NuMA$^{\Delta 22/\Delta 22}$ cells, indicating a novel function for NuMA in mitosis. Anchoring of kinetochore fibers at the spindle pole may be critical to allow Eg5 to drive initial separation of juxtaposed centrosomes. Once this occurs, overlapping antiparallel arrays of microtubules are formed between centrosomes, providing forces to drive further centrosome separation. Consistent with this interpretation, in the absence of stable kinetochore–microtubule interactions, centrosome separation after release from monopolarity is also inhibited. Thus, we provide a demonstration that Eg5-dependent centrosome separation requires the two-point attachment of microtubules at kinetochores and centrosomes.

Chromosome segregation in the absence of focused poles

The striking spindle defects observed in NuMA$^{\Delta 22/\Delta 22}$ fibroblasts did not delay progression through mitosis. Because a single unattached kinetochore is capable of delaying anaphase onset (Rieder et al., 1994), this indicates that microtubule capture by kinetochores occurs efficiently in the absence of functional NuMA. Furthermore, bulk chromosome segregation was observed to occur normally on spindles with detached centrosomes and defocused poles. These observations indicate that pole focusing is not an absolute requirement for (a) all kinetochores to be attached to spindle microtubules and (b) the bulk of chromosomes to be aligned and segregated in anaphase. Indeed, plant cells carry out faithful mitoses without centrosomes, using spindles without discernibly focused poles (Franklin and Cande, 1999). Additionally, mechanical severing of kinetochore fibers between spindle poles and kinetochores has been shown to not prevent continued poleward chromosome movements (Nicklas, 1989).

Although bulk chromosome segregation occurs normally, most NuMA$^{\Delta 22/\Delta 22}$ cells exhibited modest chromosome alignment defects, such as an elongated spindle and reduced tension across sister kinetochores. These defects are likely to result in chromosome segregation errors that explain the requirement of NuMA-dependent pole focusing for mouse embryonic viability and normal cellular proliferation. This is consistent with chromosome missegregation driving embryonic lethality (e.g., from loss of the centromere motor/tether CENP-E; Putkey et al., 2002). Alternatively, the early lethality of NuMA$^{\Delta 22/\Delta 22}$ embryos may result from missegregation of centrosomes or centrioles as spindle cargo (Pickett-Heaps 1969), which are not required for mitotic spindle function but are essential for normal embryonic development (Chatzimeletiou et al., 2008). Therefore, our evidence collectively demonstrates that NuMA and its role in focusing spindle poles is a required component of normal mammalian mitotic progression and embryonic development.

Materials and methods

Construction of NuMA-targeted mice

A mouse 129S6/SvEvTac bacterial artificial chromosome genomic library (RPCI-22; Children's Hospital Oakland Research Institute, Oakland, CA) was screened for the NuMA gene with a probe to the largest exon of NuMA. A single clone was identified and confirmed by PCR to contain the entire NuMA gene. An 8.9-kb EcoRV–ScaI fragment containing exons 16–25 was subcloned into pBluescript (Agilent Technologies). A loxP sequence and 3′ SacII restriction site were introduced upstream of exon 22 by cloning an oligonucleotide linker into a BstEII site. A loxP-FRT-PGKNeo-FRT fragment from pK-11 (Meyers et al., 1998) was inserted downstream of exon 22. Finally, the diphtheria toxin negative selection marker (Yanagawa et al., 1999) was introduced downstream of the short homology arm. The targeting vector was linearized with NotI before electroporation into ES cells. ES cell culture and transfection was performed as described previously (Putkey et al., 2002). DNA from G418-resistant ES clones was screened using PCR and genomic DNA blotting. The probe for targeting of exon 22 was amplified from R1 ES cell DNA using primers pr13 forward (5′-TTTGGTGGTGGTTTGGTC-3′) and pr13 reverse (5′-TGATAAGCAATGCCACGG-3′). Mice, ES cells, and embryos were genotyped as shown in Fig. 1 A with primers i (5′-AACCGCATCGCAGAGTTGCAG-3′), ii (5′-ATGCTCCAGACTGCCTTGGG-3′), iii (5′-GAGGAGTGGTGGCAACAGTAG-3′), and iv (5′-GGAGGTCATTCTACTGGAAG-3′). ES clones carrying the appropriate genetic modification were injected into C57/BL6 embryos at the Transgenic Mouse and Gene Targeting Core facility (University of California, San Diego, La Jolla, CA). Pups from chimeric mice were screened by coat color, and PCR was used to identify germline transmission.

Mouse embryonic fibroblast preparation and culture

Mouse embryonic fibroblasts were prepared as previously described (Putkey et al., 2002). Primary fibroblasts were maintained and passaged in an incubator set at 10% CO_2 at 37°C and maintained at 3% O_2 by a continuous flow of nitrogen gas to increase replicative lifespan as described previously (Parrinello et al., 2003). In all experiments using primary cells, fibroblasts were grown for no more than two cumulative weeks in culture after derivation.

To induce growth arrest, MEFs were cultured to confluence and shifted to media containing 2% serum. In fibroblasts carrying the Cre-ER^{TM} transgene, 4-OHT (10 mg/ml stock in ethanol; Sigma-Aldrich) was added to a final concentration of 0.1 µM (unless otherwise indicated) to cause nuclear translocation of Cre.

Retrovirus preparation and infections

Retroviral plasmids (pBABE variants) were prepared as described previously (Shah et al., 2004). For retroviral infection of primary MEFs, cells grown in 12-well plates were washed with PBS and incubated for 15 min in a humidified incubator with retroviral supernatant mixed with 8 µg/ml polybrene (Sigma-Aldrich). Plates of cells were wrapped in parafilm and spun at 1,100 *g* for 30 min at room temperature, after which the supernatant was replaced with primary MEF media, and cells were returned to the incubator.

Preparation and analysis of DNA, RNA, and cDNA

For analysis of splicing defects in NuMA$^{Neo/+}$ cells and tissues, RNA was prepared from mouse fibroblasts using the RNeasy Mini kit (QIAGEN) and from cells and tissues using TRIZOL reagent (Invitrogen). cDNA was

Published March 2, 2009

prepared using the SuperScript III First-Strand Synthesis kit (Invitrogen). Splicing events were detected in NuMA$^{Neo/+}$ cells and tissues by PCR amplification from cDNA with primers pr4 forward (5′-GTTTCAGAGAACTCGCGGCAGG-3′) and Neo31 (5′-GGATTCATCGACTGTGGCCGGCTGGGT-3′). The C-terminal half of the NuMA cDNA was amplified from the NuMA^{+} allele as a control, using primers pr4 forward and ex24 reverse (5′-GAGGAGTGGTGGCAACAGTAG-3′). For use in qPCR, RNA from cells and tissues was treated with the RNase-Free DNase set (QIAGEN) before reverse transcription. The loss of full-length NuMA mRNA from NuMA$^{Neo/+}$ cells and tissues was measured with primers 22f.2 (5′-AACCGCATCGCAGAGTTGCAG-3′) and 23r.2 (5′-TTACGTCCTTCATGCCGGTCC-3′). Cyclophilin A was amplified as a normalizer using primers cycloA forward (5′-TTCACCTTCCCAAAGACCAC-3′) and cycloA reverse (5′-AGCACTGGAGAGAAAGGATT-3′). The degree of mRNA loss was calculated using the comparative cycle time method by normalizing the signal produced from NuMA to cyclophilin A reactions and comparing NuMA$^{Neo/+}$ and NuMA$^{+/+}$ samples.

For measurements of Cre-mediated NuMA exon 22 deletion in fibroblasts, DNA was prepared using the DNeasy Blood and Tissue kit (QIAGEN). The loss of NuMA^{flox} from genomic DNA was measured using primers 22f.4 (5′-CTTGCTCTATACAGTTGGGCC-3′) and 22 reverse (5′-GGTGGGTCTCAGAGGAAACTCG-3′). The mouse γ-actin gene was amplified as a normalizer using primers 6590 (5′-TGGATCAGCAAGCAGGAGTATG-3′) and 6591 (5′-CCTGCTCAGTCCATCTAGAAGCA-3′). Reactions were performed using 40 ng genomic DNA and the SYBR Green Supermix qPCR reagent (Bio-Rad Laboratories). The degree of excision was calculated by normalizing the signal produced from an experimental sample to the unexcised gene γ-actin and comparing experimental samples to DNA extracted from NuMA$^{+/+}$ MEFs as described previously (Pfaffl, 2001). All qPCR reactions were run using the iCycler (Bio-Rad Laboratories).

Live cell microscopy

HeLa and MEF cells were seeded onto 35-mm glass-bottom dishes (MatTek) and incubated in CO_2-independent medium (Invitrogen) supplemented as described previously (Weaver et al., 2007). Dishes were placed in a heat-controlled stage set at 37°C. Fluorescence imaging was conducted using a spinning disk confocal (McBain Instruments) attached to an inverted microscope (TE2000e; Nikon) equipped with a 60×/1.4 NA objective lens. Fluorescence excitation was controlled by Metamorph software (MDS Analytical Technologies). Z-series images were acquired using a camera (Orca-ER; Hamamatsu Photonics) at 3- or 5-min intervals. Z stacks were compiled by maximum intensity projection for presentation.

Immunofluorescence

For indirect immunofluorescence analysis of frozen tissue sections, brain and spinal cord were prepared and processed as described previously (Lobsiger et al., 2005). Antibody staining was performed overnight at room temperature. Sections were mounted on slides (Superfrost Plus; Thermo Fisher Scientific) in a solution of 0.2% gelatin in PBS, dried overnight, and covered with antifade reagent (ProLong; Invitrogen) and glass coverslips before imaging.

For immunofluorescence analysis of cultured cells, cells were grown on hydrochloric acid–washed, poly-L-lysine (Sigma-Aldrich)–coated 18-mm glass coverslips and fixed in either ice-cold methanol for 10 min (γ-tubulin and cyclin B1 staining) or 4% formaldehyde in PBS for 10 min and processed using standard conditions. DNA was visualized by staining with DAPI. Images of fixed cells were acquired using a 100× oil objective on a DeltaVision-modified inverted microscope (IX70; Olympus) using SoftWorx software (Applied Precision, LLC) and were deconvolved unless otherwise indicated. Rabbit polyclonal antibodies used in this study include anti–*Xenopus* NuMA tail (1:250; Merdes et al., 1996), anti–human NuMA tail (1:500; Gaglio et al., 1995), anti–CENP-E HpX (1:200; Yao et al., 1997), anti–lamin A/C (1:500; provided by L. Gerace, Scripps Research Institute, San Diego, CA), and anti-Mad2 (1:250).

Monoclonal antibodies used include SMI-32 (1:1,000; Sternberger Monoclonals), GTU88 (1:1,000; Sigma-Aldrich), DM1A (1:1,000; Abcam), GNS1 (1:100; Santa Cruz Biotechnology, Inc.), p150^{Glued} (1:100; BD), and 5F9 (1:500; Taylor et al., 2001). These antibodies identify neurofilaments, γ-tubulin, α-tubulin, cyclin B1, dynein complex component p150^{Glued}, and BubR1, respectively. Additionally, antibodies isolated from human autoantiserum available as anticentromeric antibodies (1:100; Antibodies Inc.) were used to identify kinetochores. Secondary antibodies (Jackson ImmunoResearch Laboratories) labeled with FITC, Texas red, or Cy3 were used at final dilutions of 1:200.

Online supplemental material

Fig. S1 shows the expression pattern of NuMA in mouse tissues and the localization of NuMA in adult mouse neurons. Fig. S2 provides data characterizing the localization of GFP-tagged NuMA tail fragments. Fig. S3 provides data demonstrating splicing defects underlying hypomorphic expression from the NuMA^{Neo} allele. Fig. S4 provides additional data characterizing the phenotype of NuMA$^{\Delta 22/\Delta 22}$ cells, including timing of centrosome detachment, dynactin localization, and kinetochore fiber stability. Fig. S5 includes data that characterize VAchT-Cre transgenic mice and show the phenotype of animals with deletion of NuMA exon 22 in motor neurons. Videos 1 and 2 illustrate spindle formation and integrity throughout mitosis in cycling NuMA$^{+/\Delta 22}$ and NuMA$^{\Delta 22/\Delta 22}$ primary fibroblasts. Videos 3 and 4 show mitotic spindle structure and centrosome positioning during recovery from STLC-induced monopolarity in NuMA$^{+/\Delta 22}$ and NuMA$^{\Delta 22/\Delta 22}$ primary fibroblasts. Online supplemental material is available at http://www.jcb.org/cgi/content/full/jcb.200810091/DC1.

We thank A. Desai and K. Oegema for helpful comments and access to imaging equipment. We also acknowledge members of the Cleveland laboratory for invaluable support and helpful discussion throughout the duration of this work.

This work was supported by a grant (GM29513) from the National Institutes of Health to D.W. Cleveland, who receives salary support from the Ludwig Institute for Cancer Research. A.J. Holland is supported by a European Molecular Biology Organization Long-Term Fellowship.

Submitted: 14 October 2008
Accepted: 4 February 2009

Note added in proof. Since the final submission of this manuscript, an independent study also identified a role of kinetochore-dependent forces in prometaphase centrosome separation (Toso et al., 2009).

References

Chang, W., J.N. Dynek, and S. Smith. 2005. NuMA is a major acceptor of poly(ADP-ribosyl)ation by tankyrase 1 in mitosis. *Biochem. J.* 391:177–184.

Chatzimeletiou, K., E.E. Morrison, N. Prapas, Y. Prapas, and A.H. Handyside. 2008. The centrosome and early embryogenesis: clinical insights. *Reprod. Biomed. Online.* 16:485–491.

Cheeseman, I.M., and A. Desai. 2005. A combined approach for the localization and tandem affinity purification of protein complexes from metazoans. *Sci. STKE.*

Compton, D.A. 1998. Focusing on spindle poles. *J. Cell Sci.* 111(Pt 11):1477–1481.

Dasso, M. 2001. Running on Ran: nuclear transport and the mitotic spindle. *Cell.* 104:321–324.

Elbashir, S.M., J. Harborth, W. Lendeckel, A. Yalcin, K. Weber, and T. Tuschl. 2001. Duplexes of 21-nucleotide RNAs mediate RNA interference in cultured mammalian cells. *Nature.* 411:494–498.

Franklin, A.E., and W.Z. Cande. 1999. Nuclear organization and chromosome segregation. *Plant Cell.* 11:523–534.

Gaglio, T., A. Saredi, and D.A. Compton. 1995. NuMA is required for the organization of microtubules into aster-like mitotic arrays. *J. Cell Biol.* 131:693–708.

Gaglio, T., M.A. Dionne, and D.A. Compton. 1997. Mitotic spindle poles are organized by structural and motor proteins in addition to centrosomes. *J. Cell Biol.* 138:1055–1066.

Ganem, N.J., and D.A. Compton. 2006. Functional roles of poleward microtubule flux during mitosis. *Cell Cycle.* 5:481–485.

Gonczy, P., S. Pichler, M. Kirkham, and A.A. Hyman. 1999. Cytoplasmic dynein is required for distinct aspects of MTOC positioning, including centrosome separation, in the one cell stage *Caenorhabditis elegans* embryo. *J. Cell Biol.* 147:135–150.

Gordon, M.B., L. Howard, and D.A. Compton. 2001. Chromosome movement in mitosis requires microtubule anchorage at spindle poles. *J. Cell Biol.* 152:425–434.

Goshima, G., F. Nedelec, and R.D. Vale. 2005. Mechanisms for focusing mitotic spindle poles by minus end–directed motor proteins. *J. Cell Biol.* 171:229–240.

Gruss, O.J., and I. Vernos. 2004. The mechanism of spindle assembly: functions of Ran and its target TPX2. *J. Cell Biol.* 166:949–955.

Harborth, J., K. Weber, and M. Osborn. 1995. Epitope mapping and direct visualization of the parallel, in-register arrangement of the double-stranded coiled-coil in the NuMA protein. *EMBO J.* 14:2447–2460.

Harborth, J., J. Wang, C. Gueth-Hallonet, K. Weber, and M. Osborn. 1999. Self assembly of NuMA: multiarm oligomers as structural units of a nuclear lattice. *EMBO J.* 18:1689–1700.

Haren, L., and A. Merdes. 2002. Direct binding of NuMA to tubulin is mediated by a novel sequence motif in the tail domain that bundles and stabilizes microtubules. *J. Cell Sci.* 115:1815–1824.

Hayashi, S., and A.P. McMahon. 2002. Efficient recombination in diverse tissues by a tamoxifen-inducible form of Cre: a tool for temporally regulated gene activation/inactivation in the mouse. *Dev. Biol.* 244:305–318.

Heald, R., R. Tournebize, T. Blank, R. Sandaltzopoulos, P. Becker, A. Hyman, and E. Karsenti. 1996. Self-organization of microtubules into bipolar spindles around artificial chromosomes in *Xenopus* egg extracts. *Nature.* 382:420–425.

Heald, R., R. Tournebize, A. Habermann, E. Karsenti, and A. Hyman. 1997. Spindle assembly in *Xenopus* egg extracts: respective roles of centrosomes and microtubule self-organization. *J. Cell Biol.* 138:615–628.

Kalab, P., K. Weis, and R. Heald. 2002. Visualization of a Ran-GTP gradient in interphase and mitotic *Xenopus* egg extracts. *Science.* 295:2452–2456.

Kalab, P., A. Pralle, E.Y. Isacoff, R. Heald, and K. Weis. 2006. Analysis of a RanGTP-regulated gradient in mitotic somatic cells. *Nature.* 440:697–701.

Kapitein, L.C., E.J. Peterman, B.H. Kwok, J.H. Kim, T.M. Kapoor, and C.F. Schmidt. 2005. The bipolar mitotic kinesin Eg5 moves on both microtubules that it crosslinks. *Nature.* 435:114–118.

Khodjakov, A., R.W. Cole, B.R. Oakley, and C.L. Rieder. 2000. Centrosome-independent mitotic spindle formation in vertebrates. *Curr. Biol.* 10:59–67.

Khodjakov, A., L. Copenagle, M.B. Gordon, D.A. Compton, and T.M. Kapoor. 2003. Minus-end capture of preformed kinetochore fibers contributes to spindle morphogenesis. *J. Cell Biol.* 160:671–683.

Lewandoski, M., K.M. Wassarman, and G.R. Martin. 1997. Zp3-cre, a transgenic mouse line for the activation or inactivation of loxP-flanked target genes specifically in the female germ line. *Curr. Biol.* 7:148–151.

Lobsiger, C.S., M.L. Garcia, C.M. Ward, and D.W. Cleveland. 2005. Altered axonal architecture by removal of the heavily phosphorylated neurofilament tail domains strongly slows superoxide dismutase 1 mutant-mediated ALS. *Proc. Natl. Acad. Sci. USA.* 102:10351–10356.

Mahoney, N.M., G. Goshima, A.D. Douglass, and R.D. Vale. 2006. Making microtubules and mitotic spindles in cells without functional centrosomes. *Curr. Biol.* 16:564–569.

Maiato, H., C.L. Rieder, and A. Khodjakov. 2004. Kinetochore-driven formation of kinetochore fibers contributes to spindle assembly during animal mitosis. *J. Cell Biol.* 167:831–840.

Merdes, A., and D.W. Cleveland. 1998. The role of NuMA in the interphase nucleus. *J. Cell Sci.* 111:71–79.

Merdes, A., K. Ramyar, J.D. Vechio, and D.W. Cleveland. 1996. A complex of NuMA and cytoplasmic dynein is essential for mitotic spindle assembly. *Cell.* 87:447–458.

Merdes, A., R. Heald, K. Samejima, W.C. Earnshaw, and D.W. Cleveland. 2000. Formation of spindle poles by dynein/dynactin-dependent transport of NuMA. *J. Cell Biol.* 149:851–862.

Meyers, E.N., M. Lewandoski, and G.R. Martin. 1998. An Fgf8 mutant allelic series generated by Cre- and Flp-mediated recombination. *Nat. Genet.* 18:136–141.

Misawa, H., K. Nakata, K. Toda, J. Matsuura, Y. Oda, H. Inoue, M. Tateno, and R. Takahashi. 2003. VAChT-Cre.Fast and VAChT-Cre.Slow: postnatal expression of Cre recombinase in somatomotor neurons with different onset. *Genesis.* 37:44–50.

Nicklas, R.B. 1989. The motor for poleward chromosome movement in anaphase is in or near the kinetochore. *J. Cell Biol.* 109:2245–2255.

Parrinello, S., E. Samper, A. Krtolica, J. Goldstein, S. Melov, and J. Campisi. 2003. Oxygen sensitivity severely limits the replicative lifespan of murine fibroblasts. *Nat. Cell Biol.* 5:741–747.

Pfaffl, M.W. 2001. A new mathematical model for relative quantification in real-time RT-PCR. *Nucleic Acids Res.* 29:e45.

Pickett-Heaps, J. 1969. The evolution of the mitotic apparatus: an attempt at comparative ultrastructural plant cytology in dividing plant cells. *Cytobios.* 3:257–280.

Putkey, F.R., T. Cramer, M.K. Morphew, A.D. Silk, R.S. Johnson, J.R. McIntosh, and D.W. Cleveland. 2002. Unstable kinetochore-microtubule capture and chromosomal instability following deletion of CENP-E. *Dev. Cell.* 3:351–365.

Rieder, C.L., A. Schultz, R. Cole, and G. Sluder. 1994. Anaphase onset in vertebrate somatic cells is controlled by a checkpoint that monitors sister kinetochore attachment to the spindle. *J. Cell Biol.* 127:1301–1310.

Rodriguez, C.I., F. Buchholz, J. Galloway, R. Sequerra, J. Kasper, R. Ayala, A.F. Stewart, and S.M. Dymecki. 2000. High-efficiency deleter mice show that FLPe is an alternative to Cre-loxP. *Nat. Genet.* 25:139–140.

Shah, J.V., E. Botvinick, Z. Bonday, F. Furnari, M. Berns, and D.W. Cleveland. 2004. Dynamics of centromere and kinetochore proteins; implications for checkpoint signaling and silencing. *Curr. Biol.* 14:942–952.

Skoufias, D.A., S. DeBonis, Y. Saoudi, L. Lebeau, I. Crevel, R. Cross, R.H. Wade, D. Hackney, and F. Kozielski. 2006. S-trityl-L-cysteine is a reversible, tight binding inhibitor of the human kinesin Eg5 that specifically blocks mitotic progression. *J. Biol. Chem.* 281:17559–17569.

Soriano, P. 1999. Generalized lacZ expression with the ROSA26 Cre reporter strain. *Nat. Genet.* 21:70–71.

Taylor, S.S., D. Hussein, Y. Wang, S. Elderkin, and C.J. Morrow. 2001. Kinetochore localisation and phosphorylation of the mitotic checkpoint components Bub1 and BubR1 are differentially regulated by spindle events in human cells. *J. Cell Sci.* 114:4385–4395.

Toso, A., J.R. Winter, A.J. Garrod, A.C. Amaro, P. Meraldi and A.D. McAinsh. 2009. Kinetochore-generated pushing forces separate centrosomes during bipolar spindle assembly. *J. Cell Biol.* 184:365–372.

Tulu, U.S., C. Fagerstrom, N.P. Ferenz, and P. Wadsworth. 2006. Molecular requirements for kinetochore-associated microtubule formation in mammalian cells. *Curr. Biol.* 16:536–541.

Weaver, B.A., A.D. Silk, C. Montagna, P. Verdier-Pinard, and D.W. Cleveland. 2007. Aneuploidy acts both oncogenically and as a tumor suppressor. *Cancer Cell.* 11:25–36.

Yanagawa, Y., T. Kobayashi, M. Ohnishi, T. Kobayashi, S. Tamura, T. Tsuzuki, M. Sanbo, T. Yagi, F. Tashiro, and J. Miyazaki. 1999. Enrichment and efficient screening of ES cells containing a targeted mutation: the use of DT-A gene with the polyadenylation signal as a negative selection maker. *Transgenic Res.* 8:215–221.

Yang, C.H., and M. Snyder. 1992. The nuclear-mitotic apparatus protein is important in the establishment and maintenance of the bipolar mitotic spindle apparatus. *Mol. Biol. Cell.* 3:1259–1267.

Yao, X., K.L. Anderson, and D.W. Cleveland. 1997. The microtubule-dependent motor centromere-associated protein E (CENP-E) is an integral component of kinetochore corona fibers that link centromeres to spindle microtubules. *J. Cell Biol.* 139:435–447.

Published March 2, 2009

Supplemental Material

JCB

Silk et al., http://www.jcb.org/cgi/content/full/jcb.200810091/DC1

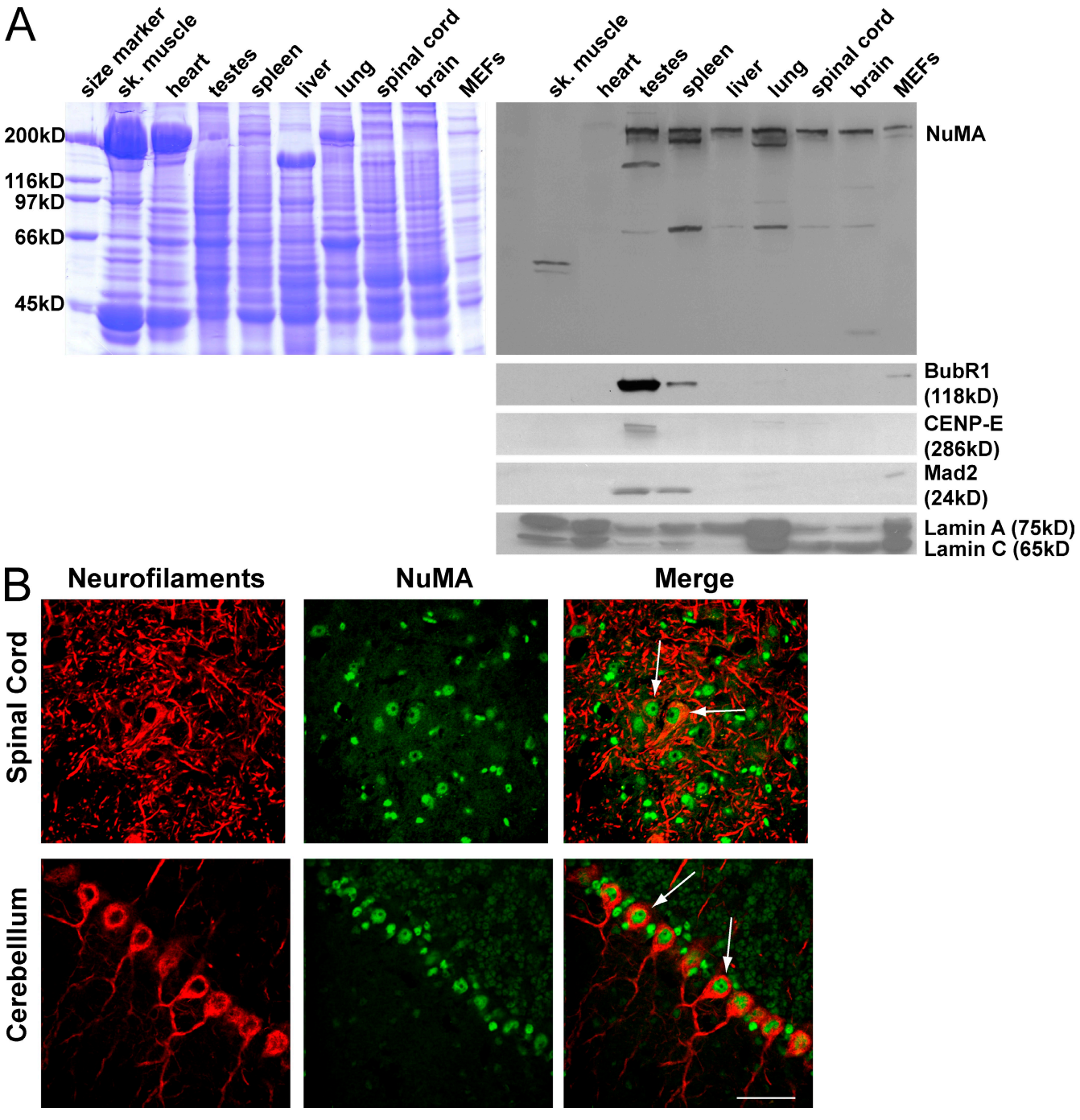

Figure S1. **NuMA is broadly expressed in mouse tissues and present in nuclei of postmitotic neurons.** (A) Coomassie-stained gel of tissue lysates from an adult C57/B6 mouse and corresponding immunoblot with antibodies to NuMA, BubR1, CENP-E, Mad2, and lamins A and C. NuMA immunoreactive bands smaller than 230 kD may represent isoforms or indicate posttranslational processing. (B) Immunofluorescence staining of frozen spinal cord and cerebellar sections from an adult C57/B6 mouse. NuMA is shown in green, and unphosphorylated neurofilaments are shown in red. Arrows indicate examples of NuMA-positive motor neurons in the spinal cord and Purkinje cells in the cerebellum. Sk muscle, skeletal muscle. Bar, 50 μm.

Published March 2, 2009

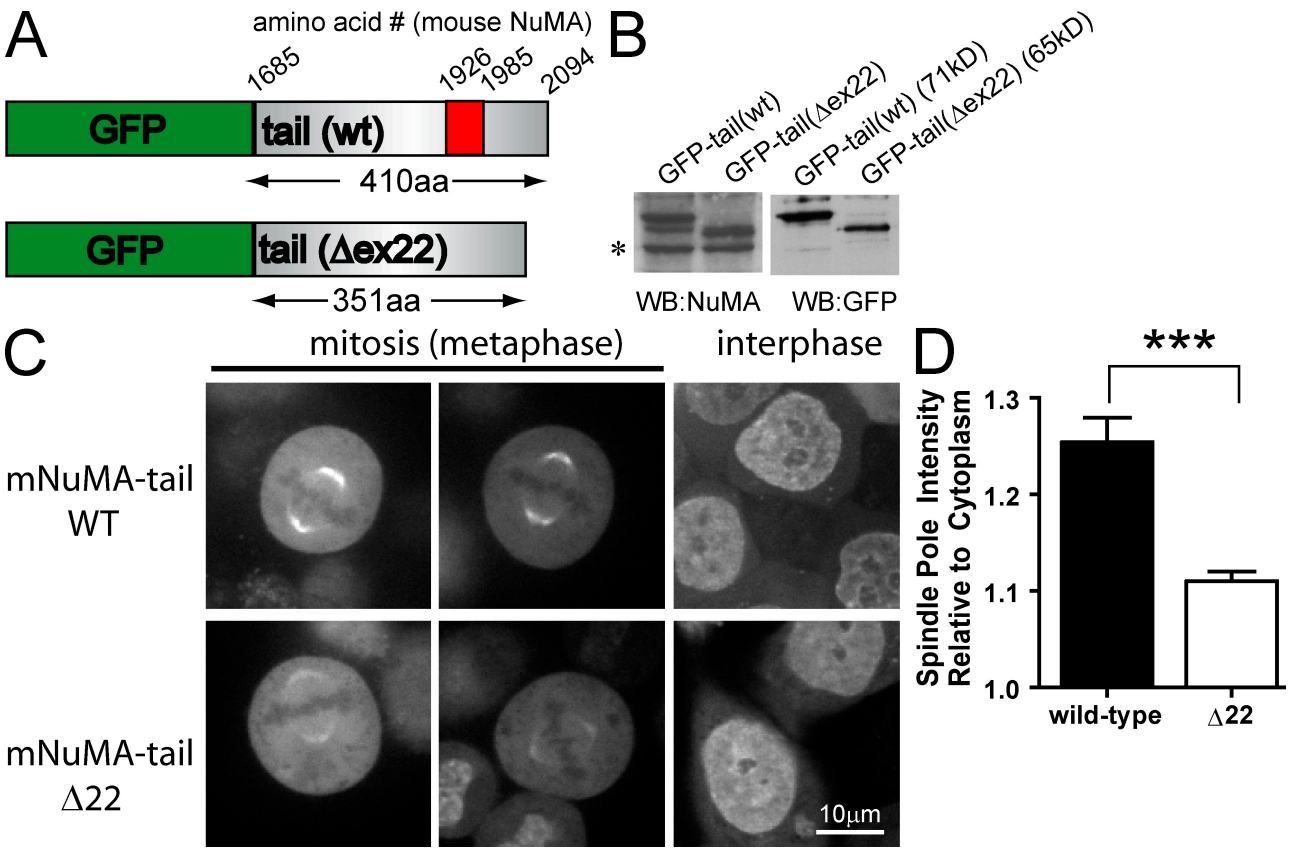

Figure S2. **Efficient spindle pole localization of mouse NuMA requires amino acids encoded by exon 22.** (A) Schematic of proteins expressed from constructs encoding either wild-type (tail [wt]) or exon 22–deleted (tail [Δex22]) C-terminal fragments of mouse NuMA (mNuMA). Amino acid numbers corresponding to mouse NuMA protein are indicated. The region encoded by exon 22 is colored in red. (B) Immunoblot of cells expressing wild-type or exon 22–deleted tail fragments probed with antibodies to GFP and NuMA. The asterisk represents a nonspecific band recognized by the NuMA antibody. (C) Localization of proteins depicted in A in HeLa cells during mitosis or interphase. Images represent single confocal z sections taken through the center of each cell and were acquired using identical settings and exposure times and were processed and scaled identically. (D) Quantification of spindle pole fluorescence from images taken as in C of metaphase cells expressing GFP-tagged wild-type or exon 22–deleted NuMA tail. Integrated pixel intensity was measured in a 100-square pixel box at the apex of each spindle pole and normalized to an identically sized region in the cytosol behind that pole. $n \geq 14$ spindle poles per construct. ***, $P < 0.0001$ by *t* test. WB, Western blot. Error bars indicate SEM.

Published March 2, 2009

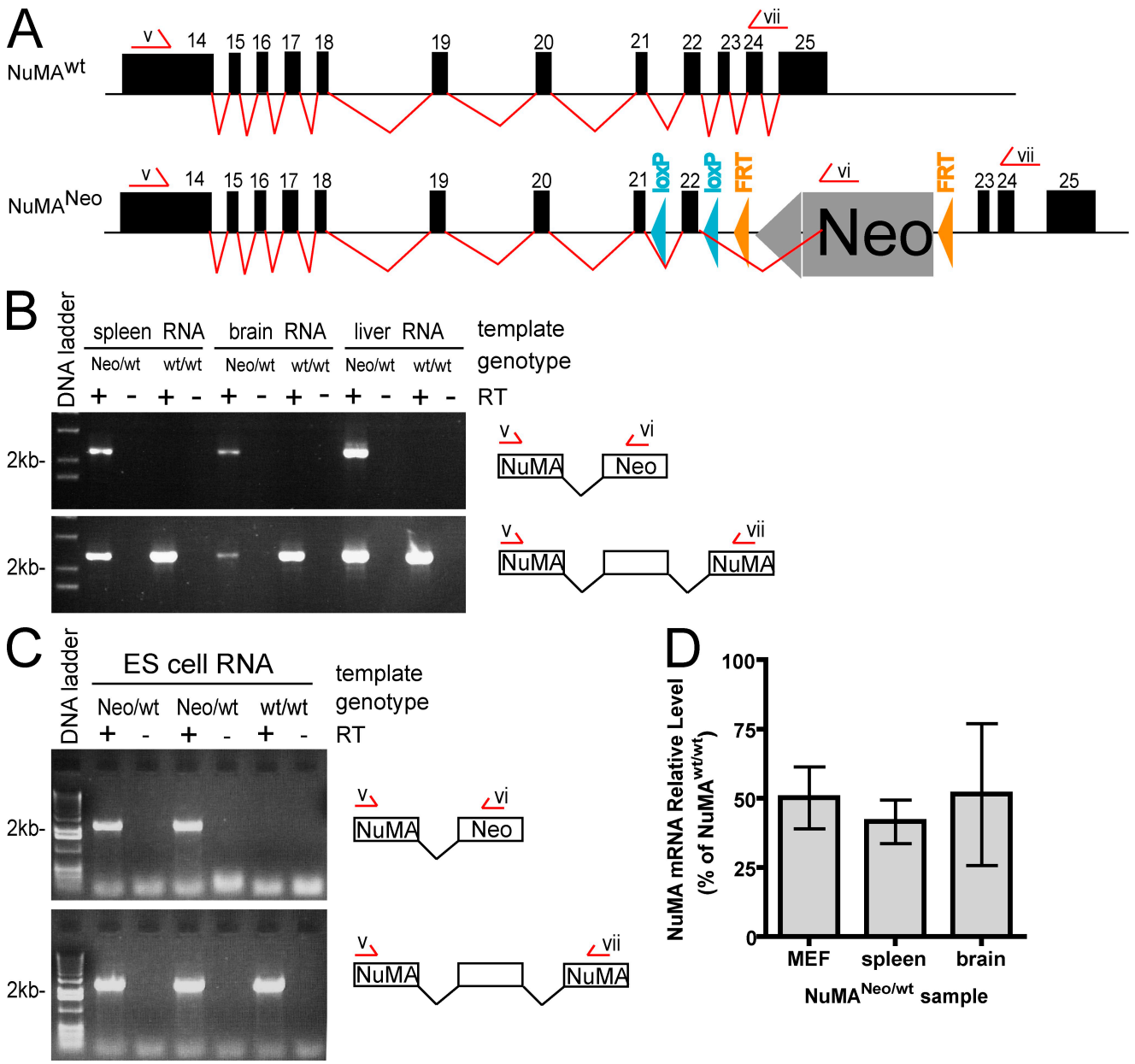

Figure S3. **Aberrant splicing disrupts expression from the NuMA^{Neo} allele.** (A) Schematic of the wild-type (NuMA^{wt}) and targeted (NuMA^{Neo}) NuMA alleles showing exons 14–25. Splicing is indicated with red connecting lines below exons, and aberrant splicing into the *Neo* cassette is indicated. Locations of PCR primers used to identify splice products (primers v, vi, and vii) are shown. (B) PCR from cDNA prepared with (+) or without (−) reverse transcription (RT) from total RNA extracted from tissues of wild-type (wt/wt) or NuMA^{Neo} heterozygous (Neo/wt) mice. Normal NuMA splicing was detected using primers v and vii, and aberrant splicing into the *Neo* cassette was detected by primers v and vi. Note that the aberrant splice product is detected only in Neo/wt + reverse transcription samples. (C) PCR as in B using total RNA prepared from homologously recombined (Neo/wt) or nonrecombinant (wt/wt) neomycin-resistant ES cell lines. (D) Quantitative PCR to determine expression of normal NuMA message in MEFs or tissues heterozygous for the NuMA^{Neo} allele. Data are plotted relative to wild-type samples. Error bars represent the mean of three experiments ± SEM.

Published March 2, 2009

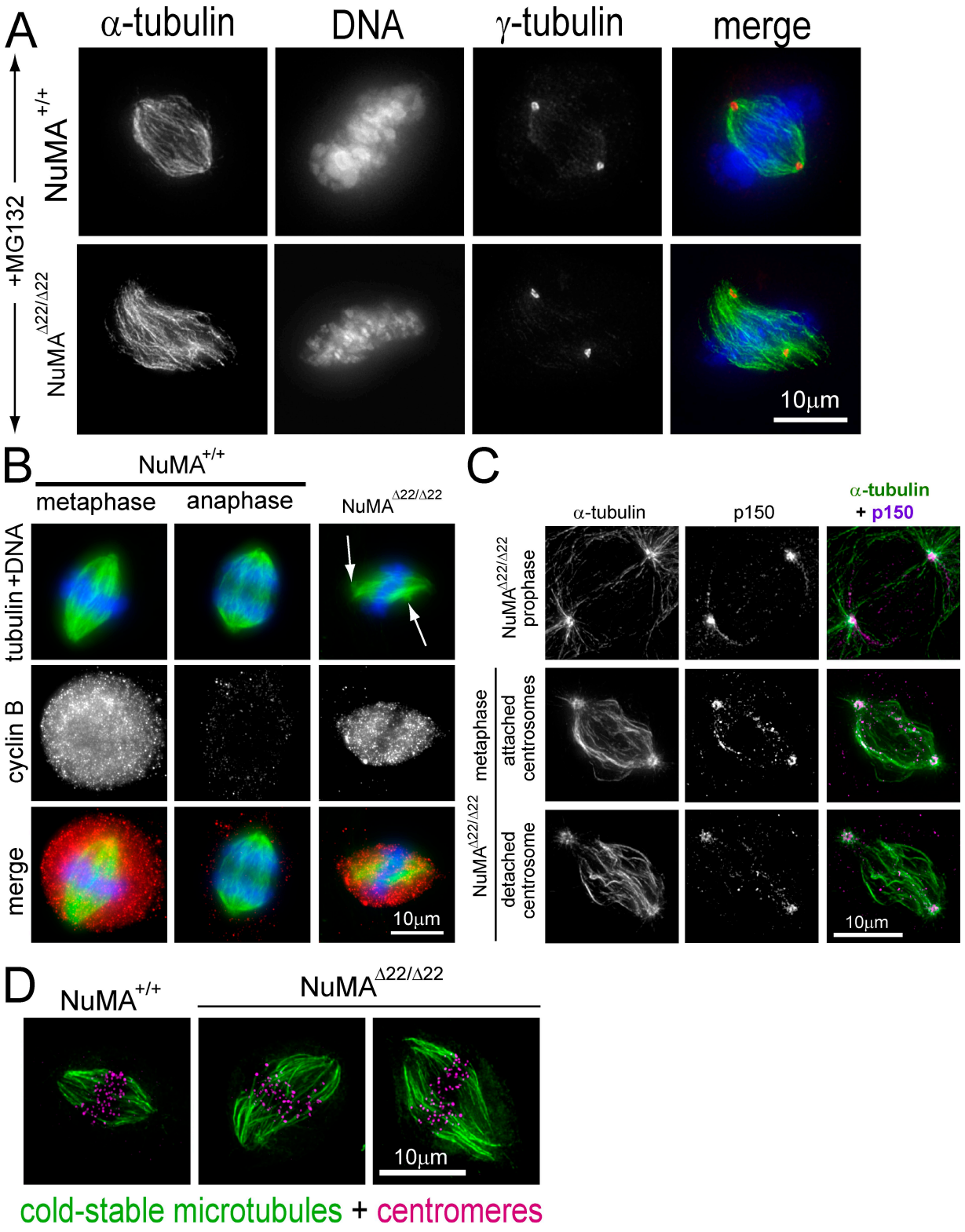

Figure S4. **Metaphase centrosome detachment with normal dynactin localization and kinetochore fiber stability in NuMA-deleted cells.** (A) Primary fibroblasts were arrested in metaphase with aligned chromosomes using MG132. In the merged image, DNA is shown in blue, α-tubulin in green, and γ-tubulin in red. Each image represents a maximum intensity projection of a deconvolved series of z sections spanning the entire cell in 0.2-μm intervals. (B) Unperturbed primary fibroblasts stained for DNA (blue), cyclin B1 to identify metaphase cells (red), and tubulin to mark spindles and centrosomes (green) are shown. Arrows indicate centrosomes. Images were acquired as in A. (C) Examples of dynein localization in NuMA$^{\Delta22/\Delta22}$ primary fibroblasts in prophase, a normal metaphase, and a metaphase figure with defocused poles and a centrosome clearly detached from the body of the spindle. In the merged image, p150 is shown in purple and α-tubulin in green. (D) Kinetochore fibers in wild-type and NuMA$^{\Delta22/\Delta22}$ cells, selectively visualized by depolymerization of unstable microtubules with a 10 min incubation at 0°C before fixation. Centromeres are marked with human ACA autoimmune antiserum (purple), and α-tubulin is shown in green.

Published March 2, 2009

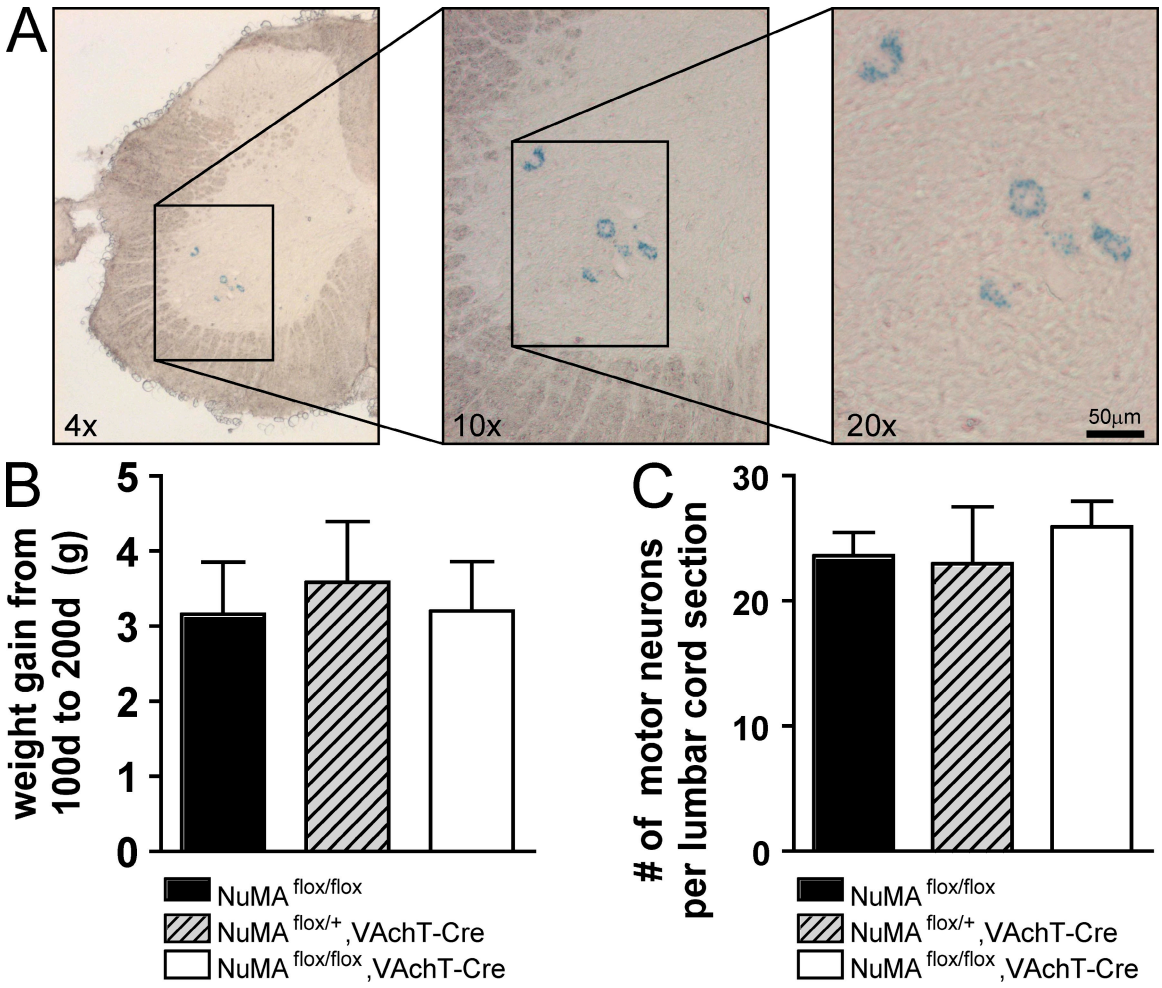

Figure S5. **Normal cellular function and viability after in vivo motor neuron–specific NuMA exon 22 deletion.** (A) X-gal staining of a spinal cord section shown at increasing magnifications from mice expressing the VAchT-Cre transgene and carrying the ROSA26R β-galactosidase reporter for Cre expression. Objective magnification is indicated in the bottom left of each image. (B) Weight gain between 100 and 200 d of age in control littermate animals and animals deleted of NuMA exon 22 in motor neurons. $n \geq 7$ animals per genotype. (C) Quantification of motor neuron numbers per 30-μm thick lumbar spinal cord section. Samples were taken from 200-d-old animals deleted of NuMA exon 22 in motor neurons and littermate controls. Three animals per genotype were examined with 15–22 spinal cord sections taken per animal. Sections were spaced ∼350 μm apart and taken through the entire lumbar spinal cord. Error bars indicate SEM.

Published March 2, 2009

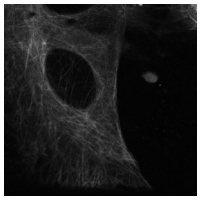

Video 1. **GFP-tubulin in a cycling NuMA$^{+/\Delta 22}$ primary fibroblast.** 5 min per frame displayed at six frames per second. Video corresponds to Fig. 4 A.

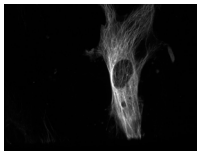

Video 2. **GFP-tubulin in a cycling NuMA$^{\Delta 22/\Delta 22}$ primary fibroblast.** 5 min per frame displayed at six frames per second. Video corresponds to Fig. 4 B.

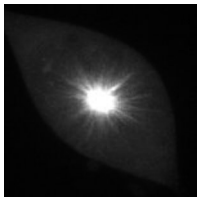

Video 3. **GFP-tubulin in a NuMA$^{+/\Delta 22}$ primary fibroblast after STLC washout.** 3 min per frame displayed at two frames per second. Video corresponds to Fig. 5 D.

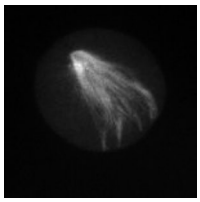

Video 4. **GFP-tubulin in a NuMA$^{\Delta 22/\Delta 22}$ primary fibroblast after STLC washout.** 3 min per frame displayed at two frames per second. Video corresponds to Fig. 5 D.